1982

Linear and nonlinear models of Mira variable stars

Dale A. Ostlie
Iowa State University

Ostlie, Dale A.

LINEAR AND NONLINEAR MODELS OF MIRA VARIABLE STARS

Iowa State University PH.D. 1982

Linear and nonlinear models of Mira variable stars

by

Dale A. Ostlie

A Dissertation Submitted to the

Graduate Faculty in Partial Fulfillment of the

Requirements for the Degree of

DOCTOR OF PHILOSOPHY

Department: Physics
Major: Astrophysics

Approved:

Signature was redacted for privacy.

In Charge of Major Work

Signature was redacted for privacy.

For the Major Department

Signature was redacted for privacy.

For the Graduate College

Iowa State University
Ames, Iowa

1982

TABLE OF CONTENTS

LIST OF FIGURES

LIST OF TABLES

I. INTRODUCTION

Since the discovery of periodic stellar luminosity changes hundreds of years ago, many kinds of variable stars have been recognized, and their properties have been studied extensively. Mira variable stars constitute a subclass of the group known as Long Period Variables. LPVs are a general class of red giant and supergiant variables with typical periods of one hundred days or more. Included are the Miras, semiregulars, and irregular variable stars. Miras may be distinguished from the other LPVs by the large amplitude of the variations in their visual magnitudes ($>2^{m}.5$, see Kukarkin et al., 1969-1976), the presence of emission lines in their spectra, and their fairly regular light curves.

Miras have been monitored regularly for over a century and are popular objects for amateur observers. As a result, large amounts of information exist concerning the periods of these stars as well as the shapes of their light curves. Unfortunately, key physical parameters of the Miras have been less well-determined: their masses, radii, luminosities, and effective temperatures are still very uncertain. Over the past few years the observational estimates of their radii, luminosities, and effective temperatures have been revised substantially, in part as a consequence of the revision of the effective temperature-color and effective temperature-spectral type relations for nonvariable red giants (Ridgway et al., 1980).

A. Observational Constraints

Observational determinations of present or progenitor Mira masses are fairly limited. The most direct technique for determining stellar masses uses visual or eclipsing spectroscopic binary systems. However, only the Miras o Ceti and X Oph are in visual binary systems for which orbits may be found. For these systems, only order-of-magnitude masses can so far be determined because their very long orbital periods ($\sim$1000 years) make it impossible to determine their orbital elements, and hence masses, with much accuracy. From preliminary calculations approximately one solar mass is indicated for both o Ceti and X Oph (Fernie and Brooker, 1961).

It has become clear that there is substantial mass loss during the evolution of a star that becomes a Mira (see section I.B). Lower limits on the progenitor masses of individual Miras may be obtained if these stars are located in binary systems with main sequence companions. If the separation of the two stars is large enough that interactions (specifically, mass transfer) do not significantly affect their evolution, then the star in the more advanced stage of evolution (in this case the Mira) must be the more massive, since more massive stars evolve more rapidly. The mass of the main sequence companion, as indicated by its spectral type, thus gives a lower limit to the mass of the Mira progenitor. Three Miras apparently having main sequence companions are AO Vir, T Sgr, and W Agl (Kukarkin et al., 1969-1976), with masses for their companions of between 1.0 $M_\odot$ and 1.7 $M_\odot$.

Further estimates of progenitor masses have been derived from population studies (Feast, 1963; Clayton and Feast, 1969) giving main sequence masses of 1.0 $M_\odot$ for the shortest period stars and more than 2.5 $M_\odot$ for those of longest period. These estimates represent upper limits on the masses of Miras due to uncertainties in the amount of mass loss that may have occurred. Atmospheric velocity structure studies (Hill and Willson, 1979; Willson, Wallerstein, and Pilachowski, 1982) imply current masses of slightly less than 1 $M_\odot$ for older (high velocity) stars and up to 2-3 $M_\odot$ for field Miras, consistent with the main sequence progenitor masses determined from population studies.

Measured values of Mira radii are strongly dependent upon the wavelength bands used and upon assumed distance scales. Angular diameters have been measured using occultations and speckle interferometry and may be as much as a factor of two larger if observations are made over broad wavelength bands at visual wavelengths rather than over narrow visual wavelength bands or in the infrared (Ridgway et al., 1977; Labeyrie et al., 1977; Tsuji, 1978; Beavers et al., 1980; Bonneau et al., 1982). Labeyrie et al. (1977) found that the measured angular diameter depends strongly on wavelength because of effects due to TiO absorption features. They have argued that the optically thick regions of the atmosphere, when measured in the TiO bands, may extend several stellar radii above the continuum forming layer. Scattering from circumstellar material may also lead to large variations in measured angular diameters (Tsuji, 1978). As a result of these effects Miras are probably smaller than previously believed.

Converting angular diameters to actual radii demands knowledge of the distances to these objects. Again the values obtained seem to depend upon the wavelengths studied and also upon the method of analysis used. Magnitudes measured in the infrared K band are apparently more consistent from star to star than are visual magnitudes (Clayton and Feast, 1969; Robertson and Feast, 1981; Willson, 1982) implying that a distance scale based on infrared magnitudes may be more appropriate than one based on visual brightnesses.

A method of determining radii from mean spectral types has also been attempted (Cahn and Wyatt, 1978; Cahn, 1980). In this approach the observed spectral type is used first to estimate the effective temperature and luminosity which, in turn, implies a radius. A comparison between theoretical pulsation models and observed periods and radii has also been used by the authors to deduce a pulsation mass if the mode of pulsation is known. This is accomplished by assuming a single theoretical Q-value defined by the relation

$$P = Q(\bar{\rho}/\bar{\rho}_{\odot})^{-1/2} \tag{1.1}$$

which is appropriate to a specific mode of pulsation. However, the pulsation "constant," Q, is generally slowly varying over a range of effective temperatures, luminosities, and masses when the mode of pulsation is specified (see Cox and Giuli, 1968).

The temperature scale for Miras has been examined a number of ways. Fits of blackbody curves to infrared energy distributions (JHKL photometry of Robertson and Feast, 1981) tend to give the lowest values, but model atmosphere calibrations of the same colors give much higher temperatures

(Willson, 1982). Detailed fitting of the energy distributions for a number of Miras over the wavelength range from 1 to 5 μm also yields higher temperatures than those found from blackbody fits (Scargle and Strecker, 1979). The same is true for $(R-I)_K$ colors (Eggen, 1975) calibrated using angular diameters (Ridgway et al., 1980) or model atmosphere calculations (Tsuji, 1978), both for nonvariable red giants.

Estimates of physical properties for Miras based on Willson (1982) are summarized in Table 1 below.

Table 1. Physical properties of Mira variable stars

Mass:	0.8 $M_\odot$[a] to 3.0 $M_\odot$[b]
Luminosity:	2000 $L_\odot$ to 10,000 $L_\odot$
Effective temperature:	3400 K ± 500 K
Radius:	150 $R_\odot$ to 350 $R_\odot$
Period:	200 days to 500 days
Absolute magnitude (M_K):	-7
Spectral type:	Me, Re, Ne, Se
Population type:	disk (old Population I)

[a]The core mass ($\sim$0.6 $M_\odot$) is an absolute lower limit.

[b]The upper bound on the mass is fairly uncertain.

B. Evolutionary Constraints

The estimated luminosities of Mira variables are larger than peak values calculated from evolutionary models for core helium burning stars (see Sweigert and Gross, 1978), indicating that Miras are probably second (or asymptotic) giant branch objects. AGB stars have already completed core helium burning and now possess a degenerate carbon-oxygen core surrounded by helium and hydrogen burning shells. Above the hydrogen burning shell is a deep convective envelope where the pulsations are believed to occur.

One characteristic feature of this phase of evolution is the existence of periodic helium shell flashes (thermal pulses). The thermal pulses repeat on time scales of 10,000 to 100,000 years and, although large surges in the rate of energy output may occur for short periods of time in the helium burning shell, only small fluctuations in the surface luminosity result (Schönberner, 1979). It has been suggested (Wood and Zarro, 1981) that these thermal pulses may be responsible for period changes in two Miras, R Hya and R Agl. Between thermal pulses (quiescent phase) the luminosity of AGB stars is due chiefly to the hydrogen burning shell.

Another important characteristic of AGB evolution is the existence of a core mass-luminosity (M_c-L) relation (see Iben and Truran, 1978), which can be used to define an inner boundary for the envelopes. This makes it possible to construct model envelopes which are compatible with realistic carbon-oxygen cores without calculating the complete core structure, thus greatly simplifying the modeling calculations.

During the Mira phase there is a strong stellar wind which dissipates much of the tenuous envelope; the Mira phase ends with the formation of a planetary nebula (Paczynski and Ziolkowski, 1968; O'Dell, 1966; Abell and Goldreich, 1966; Salpeter, 1971; Osterbrock, 1974; Wood and Cahn, 1977; Willson, 1981). Reimers (1975) gave an empirical mass loss rate for non-variable red giants expressed as

$$\dot{M} = -4 \cdot 10^{-13} \, L/g \cdot R \qquad M_\odot \, yr^{-1} \tag{1.2}$$

where L, g, and R are in solar units. For Mira variables the mass loss rates are likely to be enhanced by the effects of shock waves propagating outward through the atmospheres of these stars (Hill and Willson, 1979). Observational estimates of the mass loss rates of Miras are typically 10^{-7} $M_\odot$ yr^{-1} to 10^{-5} $M_\odot$ yr^{-1}; the mean rate of $2 \cdot 10^{-6}$ $M_\odot$ yr^{-1} (Gerhz and Woolf, 1971; Knapp et al., 1982) is still quite uncertain.

For a number of reasons, including increasing luminosity and radius and decreasing mass, the mass loss rate is expected to increase during the Mira stage. This is consistent with observed properties of these stars and with the proposal of Kwok, Purton, and Fitzgerald (1978) that a stellar wind alone may be sufficient to dissipate Mira envelopes and produce planetary nebulae. Schönberner (1981) argues that planetary nebula formation must take place during the quiescent phase but that thermal pulses may be responsible for the shells observed in some objects. This differs from previous suggestions (see Smith and Rose, 1972) that the entire production of planetary nebulae results from helium shell flashes.

Other possible mechanisms for planetary nebula formation from Miras which have been suggested include dynamical instabilities (Lucy, 1967; Paczynski and Ziolkowski, 1968; Roxburgh, 1967) and ejection of the entire envelope resulting from excessive radiation pressure (Faulkner, 1970; Sparks and Kutter, 1972). More recently the suggestion had been made that very rapid mass loss may occur as a result of severe relaxation oscillations occurring during fundamental mode pulsation in extremely low gravity models (Wood, 1974; Tuchman, Sack, and Barkat, 1979). In view of the recent upward revisions in the temperature scale, implying smaller, higher gravity stars than were previously believed, stable fundamental mode pulsation seems more likely, casting serious doubts on this last mass loss mechanism.

C. Theoretical Pulsation Studies - Literature Survey

A number of researchers have made attempts to model Mira variable stars over the past twenty years using various computer codes and approximations. In almost all cases the temperature range investigated was significantly lower (implying larger radii) than current estimates. As a result, the general conclusion of past work has been that fundamental mode pulsation produces periods which are simply too long to be associated with most Miras.

The first attempt at modeling Miras was made by Kamijo (1963a,1963b, 1963c). In that work an infinitesimal amplitude (linear), adiabatic code was used. The model of Mira calculated by Kamijo gave a fundamental mode pulsation period that was more than three times longer than observed. However, a number of weaknesses in Kamijo's study have been identified. Cox

and Guili (1968) noted that the surface boundary condition used was incorrect for the adiabatic wave equation. Langer (1969) correctly pointed out that the assumption of adiabaticity made by Kamijo in both the density variations and convective energy transport is probably invalid when dealing with Miras. Finally, Langer also noted that the assumption of instantaneous adjustment of the convective flux to local physical conditions is likely to be a very poor approximation.

In the first study of Miras using a linear, nonadiabatic pulsation code (Langer, 1969) masses from 0.7 $M_\odot$ to 2.0 $M_\odot$ were considered, as well as temperatures from log T_e = 3.322 to log T_e = 3.457 and luminosities from log $L/L_\odot$ = 3.535 to log $L/L_\odot$ = 4.115. In his study, Langer found that fundamental mode and first overtone pulsations resulted in periods which were too long to be consistent with observations then available and concluded that most Miras are probably pulsating in the second overtone.

Although Miras must be nonadiabatic pulsators, when consideration was given to changes which resulted from the inclusion of nonadiabatic effects Langer found that the pulsation periods were altered by only a few per cent. Langer also found that instantaneous adjustment of the convective flux to local physical conditions produced periods which differed little from the case where convection was not allowed to adjust at all to changing physical conditions ("frozen in"). Finally, the primary driving region for these models was found to be at the top of the hydrogen ionization zone with some additional contribution from the hydrogen molecule dissociation zone. This is different from driving due to He^+ ionization, which is characteristic of stars in the Cephid instability strip of the luminosity-effective temperature plane (the Hertzsprung-Russell or H-R diagram).

Although Langer had a number of successes in his study of the Mira region of the H-R diagram, he was careful to point out the many shortcomings of both observation and theory. In the realm of observation the important temperature scale was not well-understood, and more accurate measurements of the masses and luminosities would also have been helpful. However, Langer felt that the major weaknesses in developing an understanding of Miras were theoretical. A more realistic treatment of radiative transfer in the optically thin regions of the model envelopes is necessary because these regions may comprise a significant fraction of the stellar radius, up to 20 per cent in Langer's models, and large pulsation amplitudes are likely to exist there. Molecular opacities must be included because they can affect the rest of the structure of the envelope through changes in the surface conditions; Langer used a scheme to add water vapor opacities. However, perhaps one of the weakest links in a theoretical understanding of these stars is the convection theory used. The mixing length theory of convection used in Langer's work and still used by most researchers is a one-dimensional, free-parameter formulation without any implicit time dependence.

Keeley (1970a, 1970b) carried out the first nonlinear calculations of models for Mira variable stars. In all calculations a method of incorporating time dependence into the mixing length theory was used. In the first of his papers Keeley discussed in detail the static structure of the envelopes to be used in his dynamical calculations. In his second paper results of the nonlinear calculations are given. For one model with $M = 1.0\ M_{\odot}$, $T_e = 2600$ K, and $L = 1 \cdot 10^{37}$ ergs sec^{-1}, stable fundamental

mode pulsation occurred with a period of 300 days. In this calculation nonlocal convection equations were used, resulting in an overshoot region capable of transporting energy from the large convection zone into the convectively stable region. Keeley pointed out that this may have contributed to the stability of the oscillations. All other models studied were found to be overtone or mixed-mode pulsators.

In a study aimed primarily at exploring possible mechanisms of planetary nebula formation, Smith and Rose (1972) carried out nonadiabatic dynamical calculations related to the problem of Mira pulsations. A fundamental mode perturbation was applied to a model envelope for which M = 0.856 $M_\odot$, L = 2500 $L_\odot$, and R = 164 $R_\odot$, with pulsations of limiting amplitude apparently resulting. Although this calculation was carried through only a few pulsation periods, not far enough to determine whether the oscillations would relax to a steady state, and shock waves did develop each period, the peak kinetic energy was fairly constant and no mass loss occurred. In a second calculation with M = 0.856 $M_\odot$, L = 3984 $L_\odot$, and R = 228.2 $R_\odot$, significantly different behavior resulted. Two large-amplitude oscillations occurred early in the calculation, resulting in a shock wave that ejected 0.5 per cent of the stellar mass. After settling down to nearly hydrostatic (but not thermal) equilibrium, pulsations of rapidly increasing amplitude developed before the calculation was terminated. Smith and Rose concluded that a rapid transition to very nonadiabatic motion occurs as the luminosity increases. Unfortunately, the question of whether an entire stellar envelope may be ejected by pulsations could not be answered.

Wood (1974) raised serious questions about the possibility of steady state behavior for fundamental mode pulsations in red giant envelopes. In his work the dynamical behavior of four model envelopes was considered. Each model had $M = 0.9\ M_{\odot}$, but the luminosities ranged from $\log L/L_{\odot} = 3.415$ to $\log L/L_{\odot} = 4.142$ and the temperatures from $\log T_e = 3.412$ to $\log T_e = 3.440$. The contribution of water vapor to the opacity was calculated with a method suggested by Paczynski (1969); the mixing length theory of convection was used, but with a formalism for calculating non-local, time dependent effects; and care was taken to fit the model envelopes to realistic cores.

In discussing the static structure of the model envelopes, Wood pointed out the decrease in β (the ratio of gas pressure to total pressure) as the luminosity increased. For his most luminous model, Wood found a convective envelope supported almost entirely by radiation pressure. The onset of convection was abrupt near the top of the hydrogen ionization zone for all models and extended inward through almost the entire stellar radius.

The lowest luminosity model in Wood's dynamical calculations ($\log L/L_{\odot} = 3.415$) was found to pulsate steadily in the first overtone with a node near the middle of the hydrogen ionization zone. Two strong dissipation regions were found, one at the surface and one at the base of the envelope. Driving regions existed in the portion of the hydrogen ionization zone interior to the node and in the outer parts of the convection zone where material was moving into and out of the zone. Wood compared this model having a 146 day period to the Mira variable, S Carinae (150 days), and found qualitative agreement. However, as he pointed out, the observational estimate for the effective temperature of S Car is about 600 K

greater than his theoretical model, and the metal abundance used in his model was larger than expected for such a high velocity star.

In the nonlinear calculations of his other model envelopes, Wood found no direct comparisons to Mira variable stars. In his second model ($\log T_e$ = 3.419, $\log L/L_\odot$ = 3.604), fundamental mode pulsation dominated but was unstable; a large collapse of the envelope occurred, and the resulting rebound caused loss of a substantial amount (3.1 per cent) of stellar mass. In the other two models, both with luminosities larger than model 2, aperiodic behavior also occurred leading to severe relaxation oscillations and mass loss in the most luminous case. Wood concluded from his calculations that his overtone pulsator gave results that were consistent with the observational features of Mira variable stars. He further suggested that when some critical luminosity is exceeded, fundamental mode pulsation begins, with resulting severe relaxation oscillations. These relaxation oscillations may lead to extensive mass loss on a very short time scale and fundamental mode pulsation cannot, therefore, be associated with Miras.

In a series of papers dealing with dynamical and pulsational instabilities Tuchman, Sack, and Barkat (1978; Tuchman, Sack, and Barkat, 1979; Barkat and Tuchman, 1980; hereafter referred to as TSB) studied the behavior of a number of red giant envelopes. In the first of these papers the region of dynamical instability in the H-R diagram was investigated and found to have not only a lower luminosity limit but also an upper luminosity limit, as well as a high temperature bound. Mass loss was found to occur for stars located in the dynamical instability "well," but evolution through the region resulted in cessation of mass loss before dissipation of the entire envelope.

In the second paper of TSB, model envelopes for stars of 1 $M_\odot$ to 6 $M_\odot$ were tested for pulsational stability with luminosities lower than those considered in the first paper; the effective temperatures of these models ranged from 2250 K to 2580 K and the luminosities from 1800 $L_\odot$ to 35000 $L_\odot$. In results similar to those of Wood (1974), TSB found that below a critical luminosity (L^M) the mode of pulsation was higher than first overtone, with the amplitude being too small and irregular to be identified with Miras. Above L^M, but below a second luminosity (L^{PN}), first overtone pulsation resulted in Mira-like pulsations. As the luminosity of the model sequence was increased the contribution of the fundamental mode became more significant until, above L^{PN}, the fundamental mode dominated, with severe relaxation oscillations producing mass loss ($\sim$3 per cent) at semi-periodic intervals. TSB argued that this repetitive mass loss would produce a planetary nebula, thus ending the Mira phase even before the onset of dynamical instability.

Most recently, Fox and Wood (1982) have studied linear, nonadiabatic red giant model envelopes believed to be appropriate for the AGB. As a definition of the AGB, Fox and Wood used the (M_{bol}, R-I) relation of Eggen (1975) based on data for old disk population nonvariable giant stars. Conversion to the (log $L/L_\odot$, log T_e) plane was accomplished by adopting a specific temperature scale. For the "standard" AGB the Ridgway et al. (1980) scale, based on near IR occulation angular diameters for nonvariable red giants, was adopted. A second, cooler temperature scale (Johnson, 1966) more nearly coincident with blackbody temperatures (Robertson and Feast, 1981; Glass and Feast, 1981) was also investigated.

In their analysis of pulsation growth rates, Fox and Wood found that the first overtone is likely to dominate in the linear regime for low luminosities, with the fundamental mode dominating as the luminosity increases along the AGB. Although this study is valid only in the linear regime, the suggestion is made that the change in growth rates may be indicative of a mode switch from first overtone to fundamental mode pulsation. Based upon previous nonlinear calculations (Wood, 1974; TSB, 1979) this mode switch may indicate the onset of planetary nebula formation. Fox and Wood concluded that Miras are likely to be pulsating in the first overtone if the black body temperature scale is correct but could be fundamental mode pulsators if the Ridgway et al. (1980) scale is correct.

D. Motivation for the Present Study

All theoretical studies of Miras carried out thus far have involved assumptions that affect the results significantly. The observational determinations of mass, luminosity, and effective temperature (particularly the latter) have been substantially revised in recent years, changing the region of the H-R diagram needing examination. The smaller, hotter stars now suggested by observation are more likely to have stable fundamental mode oscillations instead of overtone modes, and this question needs to be resolved so that we will have a clear picture of the stars' structure and behavior. However, remaining uncertainties in physical parameters suggests the need for a general survey of the entire instability region of the H-R diagram.

In addition to the mode controversy the study of Miras is important for other reasons as well. It now appears likely that these stars do not simply represent a class of "odd" variables but may be the final red giant stage of evolution for all single stars of intermediate mass (Willson, 1981). As such they deserve our attention if we hope to fully understand stellar evolution in this mass range (1 $M_\odot$ to $\sim$3 $M_\odot$), containing more than 99 per cent of all stars of mass greater than 1 $M_\odot$.

Miras also present us with an opportunity to study some important and challenging astrophysics. Weaknesses in the present state of convection theory can play a significant role in the development of realistic pulsation models since convection is the dominate energy transport mechanism throughout most of the volume of these stars. The contribution of molecules to the opacity can influence the structure of the cool, outer regions as can the approximation of diffusive radiation transport throughout optically thin zones. When nonlinear oscillations are considered, assumptions inherent in the surface boundary conditions, such as mechanical energy transport beyond the outermost zone, may affect the amplitudes obtained and perhaps even mode stability.

Although all of the problems cannot be solved at this time, a number of improvements have been incorporated in the present linear and nonlinear pulsation analysis of red giant envelopes. Attempts have been made to alleviate some of the shortcomings of the mixing length theory of convection: an opacity averaging of rising and falling convective elements within a zone has been added, as well as a time dependent modulation of convective velocities during pulsation; the effects of turbulent pressure have also been investigated. Molecular opacities have been included in

all cases, and efforts have been made to follow the structure of red giant model atmospheres through the optically thin outer layers of the envelopes calculated in this study. Special care has also been taken to fit the model envelopes to realistic cores, using a theoretical core mass-luminosity relation.

In Chapter II, details of the physics used to construct the model envelopes and carry out the pulsation analyses will be presented, with some emphasis given to special features of the present work. Chapter III will involve a discussion of the hydrostatic models along with the results of the linear, nonadiabatic survey of the instability region. In Chapter IV, the nonlinear behavior of several selected models will be described and Chapter V will summarize the present work with suggestions for further study.

II. PHYSICAL CONSIDERATIONS

The theory of stellar structure has been studied extensively over the years, as have the mechanisms of pulsation in many classes of stars. The variable stars most thoroughly examined are the Cepheids and RR Lyraes, where the cause of pulsation is felt to be understood. For these stars the pulsations are due primarily to He^+ ionization at a critical depth in the envelopes. During compression, energy does not go into increased thermal motion but results in ionization instead, producing a delay in pressure and temperature elevation. After the onset of expansion, recombination releases energy capable of driving the stellar oscillations.

Unanswered questions still remain concerning these "classical" variables however. As yet no satisfactory theoretical work has been carried out to explain the return to stability at the low temperature ("red") edge of the Cepheid instability strip. This uncertainty stems from the increased effects of convection in these cooler stars and present weaknesses in the mixing length theory. Mira variable stars, which lie beyond the red edge of the Cepheid instability strip, are objects having extensive convective envelopes. This structure, as well as uncertainties in physical parameters, has resulted in a less complete theoretical understanding of the pulsation properties of Miras.

In this chapter the structure equations will be presented, together with a discussion of some important features of the physics involved. The mixing length theory of convection will be described in detail, emphasizing modifications that have been made in the standard set of equations. The boundary conditions used in both the construction of the static models and

the analysis of their time dependent behavior will be considered, and general features of the linear, nonadiabatic (LNA) and nonlinear, nonadiabatic (DYNSTAR) pulsation codes will be discussed. Both computer codes used in this study are standard stellar pulsation programs available at Los Alamos National Laboratory, but with modifications made for the present problem as described below.

A. The Equations of Stellar Structure

The equations of stellar structure for quasi-static models in thermal equilibrium have been discussed extensively in the literature (see Cox and Giuli, 1968; Clayton, 1968; Cox, 1980). These equations may be written written (assuming spherical symmetry) as

$$\frac{dP}{dr} = -\rho\frac{GM_r}{r^2} \quad \text{(hydrostatic equilibrium)} \tag{2.1a}$$

$$\frac{dM_r}{dr} = 4\pi r^2\rho \quad \text{(continuity of mass)} \tag{2.2}$$

$$\frac{dL_r}{dr} = 4\pi r^2\rho(\varepsilon_{nuc} - T\frac{dS}{dt}) \quad \text{(thermal equilibrium)} \tag{2.3}$$

$$\frac{dT}{dr} = -\frac{3}{4ac}\frac{\bar{\kappa}\rho}{T^3}\frac{L_r}{4\pi r^2} \quad \text{(radiative transport - diffusion approximation)} \tag{2.4a}$$

$$\frac{dT}{dr} = \nabla\frac{T}{P}\frac{dP}{dr} \quad \text{(convective transport)} \tag{2.4b}$$

where $\nabla \equiv \frac{d \log T}{d \log P}$ is determined from the mixing length theory. In the event that hydrostatic equilibrium is violated, as in the case of stellar pulsations or other dynamical situations, then Equation 2.1a must include an acceleration term

$$\frac{dP}{dr} = -\rho\left[\frac{GM_r}{r^2} + \frac{d^2r}{dt^2}\right] \tag{2.1b}$$

A series of constitutive relations dealing with the physical properties of the material must also be included with the mathematical equations above. These are

$$P = P(\rho, T, \text{composition}) \quad \text{(Pressure equation of state)} \tag{2.5}$$

$$E = E(\rho, T, \text{composition}) \quad \text{(Internal energy equation of state)} \tag{2.6}$$

$$\varepsilon = \varepsilon(\rho, T, \text{composition}) \quad \text{(Energy generation)} \tag{2.7}$$

$$\bar{\kappa} = \bar{\kappa}(\rho, T, \text{composition}) \quad \text{(Opacity)} \tag{2.8}$$

In order to uniquely define a stellar model, a set of boundary conditions must be specified. The usual choice of conditions for evolutionary models is

$$r = 0: \quad M_r = 0 \tag{2.9a}$$

$$L_r = 0 \tag{2.9b}$$

$$r = R_e: \quad T = T_e \tag{2.9c}$$

$$P = P_s \tag{2.9d}$$

where T_e is the effective temperature defined by

$$L = 4\pi R_e^2 \sigma T_e^4 \tag{2.10}$$

with R_e being the photospheric radius, and P_s is the pressure at R_e. When full stellar models are not calculated, as is the case here, different boundary conditions may be required; the choice of conditions used in the present study will be described in detail in Section D.2.

B. Energy Transport

1. The diffusion theory

In convectively stable regions of the model envelopes, energy transport is calculated using the diffusion theory of radiation as expressed by Equation 2.4a. Implicit in the equation are the assumptions of local thermodynamic equilibrium (LTE) and a wavelength averaged (gray) opacity. Although the diffusion approximation is good in the optically dense regions deep within a star, it becomes poor in the low density regions near the surface; care should be taken when using it in the outer zones of a stellar envelope.

2. The mixing length theory

When the temperature gradient becomes sufficiently large, energy transport is governed by convective mass motions. This form of energy transport is generally calculated by means of the Böhm-Vitense (1958) mixing length theory. In the mixing length theory a mass element which finds itself out of hydrostatic balance will either rise or fall slightly; if this displacement restores hydrostatic balance, convection will be inhibited, but if the element is then even farther from balance the region will be convectively unstable. In the latter situation the mass element will continue its motion until it "thermalizes" with its surroundings, radiating or absorbing energy until balance is obtained. The distance through which the element travels before "thermalizing" is defined as the mixing length, with the ratio of the mixing length to the pressure scale height (ℓ/H_p) considered as a free parameter ($\sim$1).

The mixing length theory is described in detail by Cox and Giuli (1968). The equations used here are:

$$\bar{V}_c = \frac{1}{4\sqrt{2}} \frac{g^{1/2} Q^{1/2} \ell}{H_P^{1/2}} f \tag{2.11}$$

$$H_c = 4\pi r^2 \frac{1}{32\sqrt{2}} \frac{g^{1/2} Q^{1/2} c_p \ell^2 \rho T}{H_P^{3/2}} f^3 \tag{2.12}$$

where

$$f \equiv [\sqrt{1 + 4 A^2 (\nabla - \nabla_{ad})} - 1]/A \tag{2.13}$$

and

$$A \equiv \frac{Q^{1/2} c_p \bar{\kappa}}{12\sqrt{2} a c} \cdot \frac{g \rho^{5/2} \ell^2}{p^{1/2} T^3} . \tag{2.14}$$

In this system of equations, $\bar{V}_c$ is the mean velocity of a convective element, $\bar{H}_c$ is the convective flux, $H_P \equiv P/\rho \cdot g$, $Q \equiv -\left.\frac{\log \rho}{\log T}\right|_P \sim 1$, ∇_{ad} is the adiabatic temperature gradient, and all other quantities have their usual meanings.

C. Pulsation Analysis

1. Linear approximation

Linear pulsation theory has been frequently discussed (see Cox, 1980) and will be described only briefly here. When analyzing the pulsational characteristics of a model envelope in the linear, nonadiabatic

regime the requirements of hydrostatic and thermal equilibrium are relaxed (i.e. $\frac{d^2r}{dt^2} \neq 0$, $T\frac{dS}{dt} \neq 0$) and small amplitude, time dependent variations of the stellar structure variables are assumed to be of the form

$$\frac{\delta\rho}{\rho} = \left(\frac{\delta\rho}{\rho}\right)_{sp} e^{i\omega t} \tag{2.15a}$$

$$= \left|\left(\frac{\delta\rho}{\rho}\right)_{sp}\right| e^{i(\omega t+\phi_\rho)} \tag{2.15b}$$

where $\left|\left(\frac{\delta\rho}{\rho}\right)_{sp}\right| << 1$ and ω is complex. After substitution into the structure equations the eigenvectors, e.g. $\left(\frac{\delta\rho}{\rho}\right)_{sp}$, and eigenvalues, ω, may be obtained for several modes. The real part of ω, $Re(\omega)$, will give the oscillation frequency while the imaginary part, $Im(\omega)$, corresponds to the rate of growth or decay of the pulsation amplitude. Details of the actual pulsation analysis used in LNA, including a discussion of the differencing scheme, may be found in Langer's (1969) work as well as in a paper by Castor (1971).

2. Full amplitude oscillations

Calculations of full amplitude, nonadiabatic stellar oscillations require time integrations of the entire set of structure equations given in Section A. DYNSTAR is an implicit pulsation code capable of carrying out such a procedure. No assumptions are made concerning the time dependent nature of the envelope structure as is done in the linear analysis.

In the hydrodynamical calculations a model is considered to have converged to an acceptable solution after a given time step only if both energy and momentum are conserved throughout the model to within a specified limit. The contributions to the energy equation considered here include changes in the internal energy content of a zone (excitation, ionization, and dissociation energies, particle kinetic energy, radiation, and in some cases, turbulent energy), mechanical work done by zonal expansion or compression (PdV work), nuclear energy sources (if any), and radiative and convective luminosity input and losses. Momentum conservation simply requires that changes in the momentum of a zone be consistent with all external forces acting on that zone.

D. Model Features

1. Composition

The composition used in all models is the Ross-Aller mixture (Ross and Aller, 1976) having (Y, Z) = (0.28, 0.02). Included are contributions from a number of molecular species, both in the equation-of-state and the opacity.

2. Boundary conditions

In the static models presented here, the stellar structure equations are integrated zone by zone beginning at the surface. Because the choice of boundary conditions uniquely defines the structure, care must be taken in their application. For the surface conditions, consideration should also be given to the breakdown of the approximation of diffusive radiation transfer through optically thin zones. For the inner boundary conditions,

the stellar envelopes calculated here need to be consistent with realistic cores even though an entire model is not actually computed.

In an attempt to minimize the errors introduced by using the diffusion theory in optically thin zones, the surface pressure and the optical depth at the center of the outermost zone were adjusted to obtain the best possible agreement with the model atmospheres of Johnson, Bernat, and Krupp (1980; hereafter JBK). These models assume LTE, are in hydrostatic equilibrium, and have neglected curvature (i.e. are plane-parallel). Unfortunately, when applied to Mira variable stars each of these approximations is poor. The existence of shocks in the atmospheres of Miras has been well documented (see Hinkle and Barnes, 1979; Willson, Wallerstein, and Pilachowski, 1982), and the very extended, tenuous atmospheres are certainly not plane-parallel. However, when applied to construction of the initial hydrostatic model envelopes only the plane-parallel approximation is likely to introduce significant errors.

The surface pressure, P_s, was adjusted by changing the amount of inertial mass assumed to lie above the outermost zone. The optical depth of the outermost zone, τ_{top}, defines the temperature in that zone through the relation

$$T_{top}^4 = \frac{3}{4} T_e^4 (\tau_{top} + \frac{2}{3}). \qquad (2.16)$$

Given P_s and τ_{top} the integration proceeds inward and is tested to be sure that $T = T_e$ at $r = R_e$. Figure 1 shows the effects on envelope structure of varying $f_a \equiv M_{IR}/M_{IR+1}$ (where M_{IR} is the mass of the outermost zone and M_{IR+1} is the inertial mass above the outermost zone) and τ_{top}. An

Figure 1. Effects of varying surface conditions on envelope structure

Models A, B, C, and D correspond to the models of Table 2. In all cases $M = 0.8\ M_{\odot}$, $L = 5000\ L_{\odot}$, $T_e = 3275$ K and $\ell/H_p = 2.5$. An extrapolated plane-parallel model atmosphere of JBK has been included for comparison.

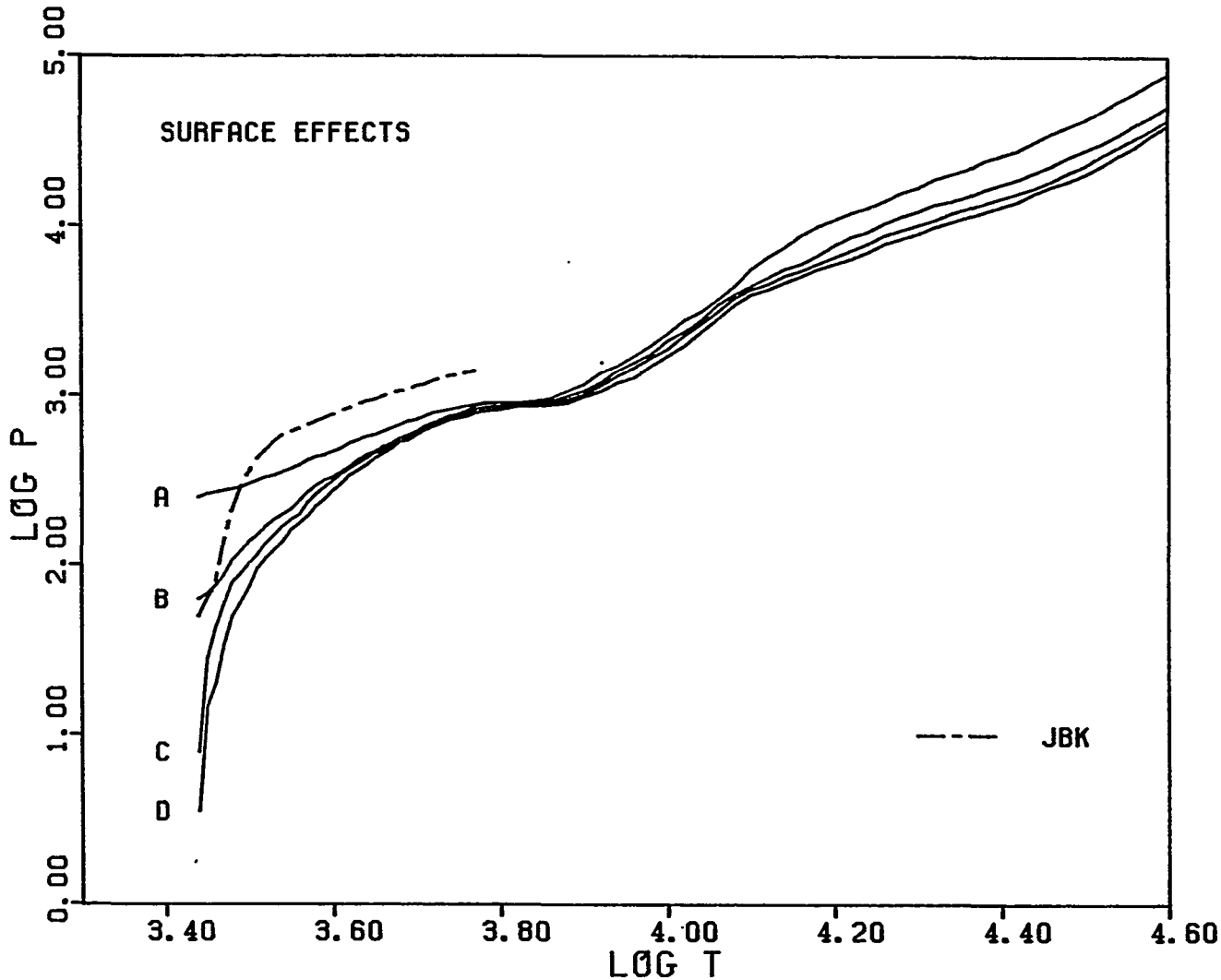
SURFACE EFFECTS
LØG P
LØG T
5.00
4.00
3.00
2.00
1.00
0.00
3.40
3.60
3.80
4.00
4.20
4.40
4.60
A
B
C
D
JBK

extrapolated model atmosphere of JBK is included for comparison. The fundamental mode nonadiabatic periods (P_o) and linear growth rates ($\eta_o \equiv \exp(P_o \cdot I_m(\omega_o))-1$) for the models of Figure 1 are given in Table 2. It is reassuring to note that although the outer structure of the envelopes changes significantly for various choices of f_a and τ_{top}, the pulsation periods and growth rates are relatively insensitive to these choices. This is probably a result of the dominance of convection in determining the temperature structure throughout most of the volume of these stars.

Table 2. The effects of f_a and τ_{top} on P_o and η_o

Model	f_a	τ_{top}	P_o(days)	η_o
a	0.01	0.01	347	2.72
b	0.005	0.001	342	3.16
c	0.01	0.001	342	3.24
d	0.1	0.001	339	3.39

After specification of the outer boundary conditions, a large (actually infinite) number of possible solutions still exist for the stellar structure equations when convective model envelopes are calculated. The selection of a particular solution results from the choice of a value for the mixing-length-to-pressure-scale-height ratio. The value of ℓ/H_p used here for a given model was chosen so that the envelope inner boundary would be consistent with the core mass-luminosity relation characteristic of AGB evolution.

The form of the M_c-L relation adopted for this study replaces Equations 2.9a and 2.9b and is given by (Iben and Truran, 1978)

$$L = 6.34 \cdot 10^4 (M_c - 0.44)(M_*/7)^{0.19} \tag{2.17}$$

where M_* is the total stellar mass, M_c is the mass of the degenerate carbon-oxygen core, and L is the total luminosity (with all variables in solar units). It should be noted that although M_c may be specified by Equation 2.17, approximately 0.1 $M_\odot$ of material lies between the C-O core and the hydrogen burning shell where the inward integrations were terminated. However, unpublished models of Iben allowed a direct comparison with some of the envelope calculations described here, and the derived periods were found to be very insensitive to small (<20 per cent) errors in the estimated inner mass.

The ability of ℓ/H_p to influence the amount of mass contained in a convective envelope may be understood by considering Equations 2.11 through 2.14. If ℓ/H_p is increased the total convective flux will remain constant (assuming all other quantities are unchanged) only if the temperature gradient becomes less superadiabatic (i.e. decreasing $\nabla-\nabla_{ad}$). This decrease means that the pressure and, therefore, the density will rise more rapidly with increasing temperature. Thus, adjusting ℓ/H_p provides a method of regulating the amount of mass located above the hydrogen burning shell.

In a related problem the effective temperatures of evolutionary tracks may be adjusted by varying the value of ℓ/H_p used (see Henyey, Vardya, and Bodenheimer, 1965). Observed red giant branches may, in this way, be

matched by the theoretical calculations. Thus, the surface conditions are determined by the selection of ℓ/H_p, with the inner boundary (the center of the star) defined by Equations 2.9a and 2.9b, as opposed to the procedure of the present study where the surface conditions are initially specified and the inner boundary (the base of the envelope) is determined by ℓ/H_p.

Additional boundary conditions are included in the pulsation analyses of LNA and DYNSTAR. In both codes motions are assumed to be negligible at the inner boundaries of the envelopes. When care is taken to locate the inner boundary near the edge of the hydrogen burning shell, this approximation introduces only small errors in pulsation periods and growth rates, as evidenced by adjustments in boundary depth. At the surface the assumption is made that all energy losses other than radiation produce insignificant changes in mode stability and in pulsation periods and amplitudes. Although this approximation is probably reasonable in the infinitesimal amplitude calculations of LNA, for the large amplitude oscillations of DYNSTAR it is a major source of uncertainty.

3. Opacity averaging

As a means of removing an inherent inconsistency in the mixing length theory a zone-by-zone averaging of the different opacities of rising and falling convective elements has been included in all models, using an adaptation of a scheme suggested by Deupree (1979). The temperature difference between a hot, rising element or a cold, falling element and the ambient temperature is estimated by making use of the expression (Cox and Giuli, 1968) for the change in temperature over one mixing length given by

$$\Delta T(\ell) = \ell \Delta \nabla T \tag{2.18}$$

where

$$\Delta \nabla T = \left(\frac{2}{\pi^2} \quad \frac{H_c^2 T}{r^4 g \rho^2 c_p^2 \ell^4 Q} \right)^{\frac{1}{2}} . \tag{2.19}$$

Using the assumption that the pressure change is a second order effect and therefore is negligible, the opacity of each element is determined and averaged according to the scheme

$$\frac{1}{\kappa} = \frac{a}{\kappa(T_o+\Delta T)} + \frac{b}{\kappa(T_o)} + \frac{c}{\kappa(T_o-\Delta T)} \tag{2.20}$$

where a, b, and c are weighting factors (with a + b + c = 1) and T_o is the average temperature of the zone. It was found that changes in the ratios of a, b, and c made very little difference in the average. This is due to the large values of $\Delta T/T$ (typically 40 per cent) in regions of the star such as the ionization zones, where the opacity is most temperature dependent. In these regions the lowest opacity element dominates the average. As a result, radiation tends to "stream" through the convective elements with the lowest opacity. Because of the small effects of varying a, b, and c, all three were arbitrarily set equal to one-third.

4. Turbulent pressure

The effects of including turbulent pressure resulting from convective motions were studied in both LNA and DYNSTAR. The form of the turbulent pressure term used is

$$P_{turb} = \tfrac{1}{2}\rho V_c^2 \tag{2.21}$$

and has been included in the expression for the temperature gradient, ∇, in selected models. Because the temperature gradient directly influences the convective velocity an iteration scheme was required to achieve a consistent solution.

5. Time dependent convection

The standard mixing length theory discussed above suffers a major flaw when used to describe convective energy transport in pulsating stars: its lack of any time dependence. In the case of Mira variable stars a typical time scale for convection, defined as the amount of time necessary for a convective element to travel one mixing length ($\tau_{conv} = \ell/V_c$) is $\tau_{conv} \sim 0.3 \cdot P_o$, where P_o is the fundamental mode pulsation period of the star. (For overtone pulsation the ratio τ_{conv}/P will be even higher.) Because of the approximately equal time scales of pulsation and convection some sort of time dependent formulation is needed.

Time dependence has been treated differently in the two pulsation codes used here. In LNA, convection is assumed to be "frozen in" and is not allowed to adapt at all to a changing environment. In view of the similarity between convection and pulsation time scales, such an assumption may not be valid. However, Langer's (1969) finding in the linear regime that pulsation periods are fairly insensitive to whether convection was "frozen in" or allowed to adjust instantaneously gives some hope that perhaps our results are not completely unrealistic.

In DYNSTAR, the convective flux is allowed to adjust to changing conditions on a time scale determined by the convective velocity. The scheme used here is similar to the method used by Wood (1974),

$$V_i^{n+1} = V_i^n + \frac{\Delta t}{\tau_i}\left(V_{o,i} - V_i^{n+1}\right) \tag{2.22}$$

where

$$\tau_i = \frac{2\ell_\tau}{V_i^n + V_i^{n+1}} \tag{2.23}$$

(but with $0 \leq \Delta t/\tau_i \leq 1$, always). In Equation 2.22, $V_{o,i}$ is the instantaneous convective velocity of zone i calculated from the mixing length theory using local conditions, V_i^n and V_i^{n+1} are the convective velocities of zone i for the time steps n and n+1, respectively, Δt is the length of the time step, and ℓ_τ is a free length parameter.

The time scale for adjustment (τ_i) is altered by changing ℓ_τ. In the limit of large ℓ_τ($\Delta t/\tau_i \sim 0$) convection becomes time independent ("frozen in") and $V_i^{n+1} = V_i^n$. If, on the other hand, ℓ_τ is small (implying $\Delta t/\tau_i \sim 1$) the assumed convective velocity is just the average of the instantaneous and previous velocities, or $V_i^{n+1} = \frac{V_{o,i} + V_i^n}{2}$. Generally ℓ_τ has been set equal to the mixing length for this study.

6. Convergence limits

All static models computed here, to be tested for pulsational stability using the linear eigenvector technique, had 150 zones and were required to converge to better than one part in 10^7 at every level for both hydrostatic

and thermal equilibrium. When static models were computed for analysis by nonlinear methods, only 60 zones were used because of time and storage constraints. In the latter case hydrostatic and thermal equilibrium was typically obtained to better than one part in 10^{12} for each zone to avoid pertubations resulting from poor convergence. At each time step in the nonlinear calculations solution of the energy and momentum equations was better than one part in 10^{7} everywhere. If, at a particular time step, convergence was not obtained within the limits specified, the time increment was decreased until a solution could be found.

III. STATIC AND LINEAR PULSATION PROPERTIES OF RED GIANT MODEL ENVELOPES

Linear, nonadiabatic models cannot yield information concerning full amplitude modal stability and time dependent behavior, but they do have the advantage that calculations for them are relatively inexpensive, so large numbers of them can be studied. Linear models can provide information about growth rates and driving mechanisms in the limit of infinitesimal oscillations. Presumably the pulsation periods obtained are similar to those of nonlinear models, as has been satisfactorily demonstrated for many "classical" variables.

For this portion of the study it was decided that a fairly large area of the red giant region of the H-R diagram should be investigated because of the uncertainties in existing observational constraints. About 100 models have been run with masses of 0.8, 1.0, 1.4, and 2.0 $M_{\odot}$ considered and with temperatures and luminosities ranging from 2700 K to 3400 K and from 1500 $L_{\odot}$ to 7000 $L_{\odot}$, respectively. Many of the models calculated may have no correlation with actual stellar objects, but it is hoped that the Mira region has been included in this survey. If this proves not to be the case perhaps a reasonable extrapolation of these results may be possible.

In all models the ratio of the mixing length to the pressure scale height has been adjusted to make the envelope mass consistent with the core mass-luminosity relation as discussed in Chapter II. Zonal opacity averaging has also been included in all cases, while turbulent pressure effects have been considered in only a small number of models.

A. Characteristics of Static Model Envelopes

All of the red giant model envelopes calculated here have similar features, with extensive convection zones dominating their structures. In this chapter an example of a typical AGB model envelope will be discussed in detail. For this "standard" model M = 1.0 $M_\odot$, L = 5000 $L_\odot$, T_e = 3000 K, and ℓ/H_P = 2.61. Effects on the structure resulting from changes in various parameters will also be described.

1. The hydrogen burning shell and the M_c-L relation

An obvious feature of the structure of AGB stars, allowing an unambiguous identification of the base of the envelope, is the on-set of hydrogen burning in a shell and the corresponding rapid rise in temperature, pressure, and density as may be seen in Figure 2. It is this feature of these models which allows the use of the M_c-L relation as an inner boundary condition. However, as was pointed out in Chapter II there is roughly 0.1 $M_\odot$ of material between the degenerate carbon-oxygen core and the top of the hydrogen burning shell. Fortunately, errors resulting from uncertainties in just how much mass exists there only very weakly influence the pulsation results.

2. Convection

At the top of the envelope a rapid inward rise in temperature exists until the onset of convection at $M_r/M_* = 0.992$. At this point even though the temperature gradient (∇) is less superadiabatic the opacity has increased significantly due to hydrogen ionization, and very efficient convection

Figure 2. Hydrostatic structure of the "standard" 1.0 $M_\odot$ model (with L = 5000 $L_\odot$, T_e = 3000 K, and ℓ/H_P = 2.6)

The maximum values obtained are log R_{max} = 13.2641, log T_{max} = 6.6618, log P_{max} = 12.6577, and log ρ_{max} = 2.2531, where the units for radius, temperature, pressure, and density are cm, degrees Kelvin, dyne cm^{-2}, and gm cm^{-3}, respectively. The inward integration was terminated at $M_r/M_* = 0.687$.

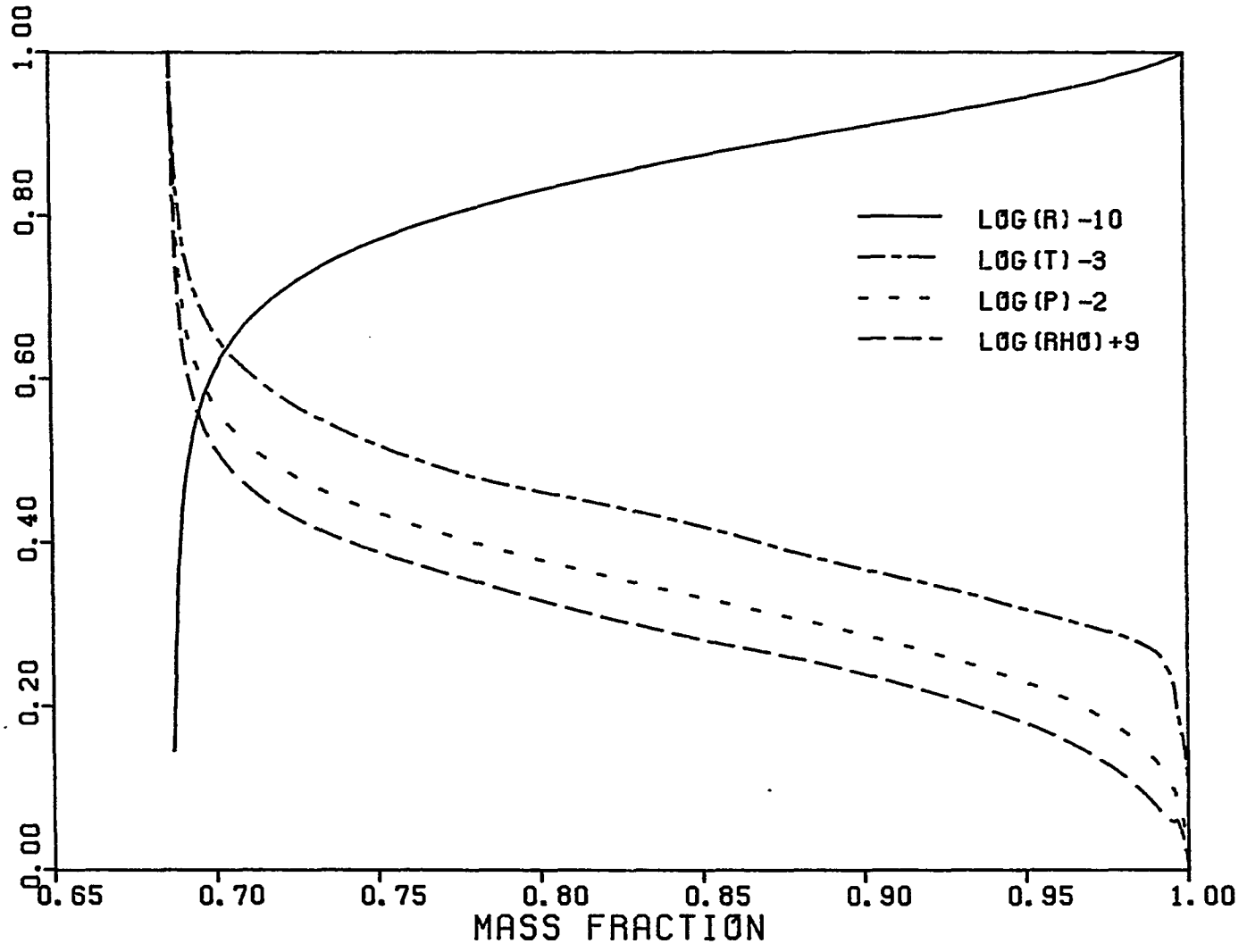
LOG(R)-10
LOG(T)-3
LOG(P)-2
LOG(RHO)+9
1.00
0.80
0.60
0.40
0.20
0.00
0.65
0.70
0.75
0.80
0.85
0.90
0.95
1.00
MASS FRACTION

results. With the addition of convective energy transport the luminosity need not be carried solely by radiation and the steep gradient is no longer required.

The location of the top of the convection zone is dependent upon the increase in opacity and is, therefore, influenced strongly by the use of the opacity averaging scheme described in Section II.D.3. Figure 3 shows the ratio of radiative-to-total luminosity as a function of temperature along with the temperature difference between rising or falling convective elements and the average zone temperature (actually $\Delta T/T$). Apparent is the rapid increase in convective luminosity for temperatures greater than 9000 K, just below the peak of $\Delta T/T$. Without the use of the opacity averaging scheme the onset of convection occurs nearer 7000 K. It is worth noting that although opacity averaging changes the static structure of these models significantly, it changes the linear pulsation periods by less than ten per cent.

Because of the strong dependence of the radiative-convective transition on temperature, adjustment of the effective temperature of the model affects the amount of mass above the convection zone. As T_e is decreased at constant luminosity (implying an increased radius) the amount of mass above the convection zone increases and a smaller fraction of the volume of the star is dominated by convective energy transport. As the luminosity or radius is increased (with the effective temperature held constant), again more mass is above the convection zone and the fraction of the volume of the star dominated by convection is smaller. Apparently the expansion of

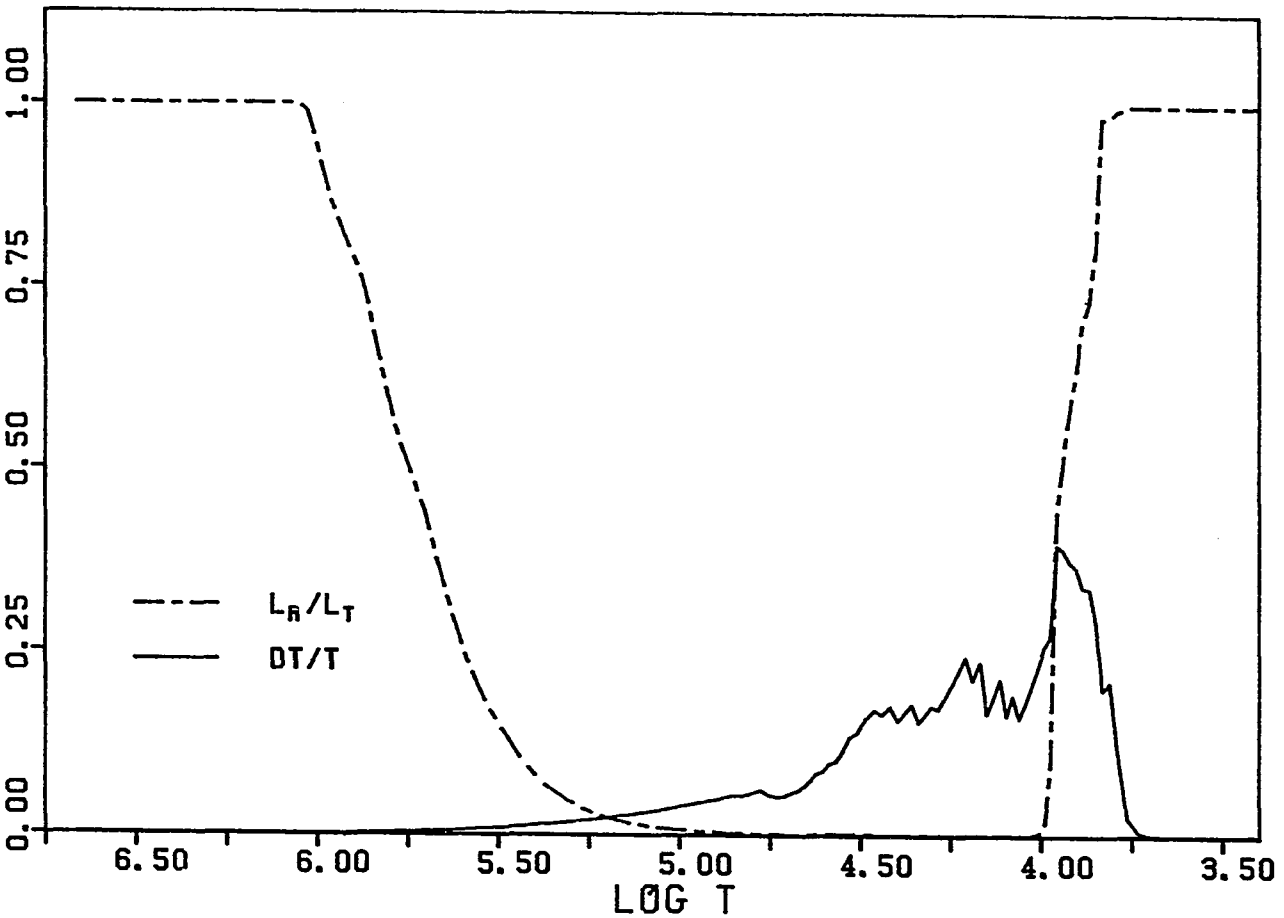

Figure 3. Radiative luminosity and the convective element temperature difference as a function of temperature

The maximum in DT/T corresponds to the top of the hydrogen ionization region where the opacity is highly temperature dependent.

the convection zone lags behind the quasi-static radial expansion of the star. The convection zone was also found to lie deeper in stars of smaller mass.

3. The density inversion

An interesting feature of the structure of red giant model envelopes is a local density maximum near the surface ($M_r/M_* = 0.996$ in the "standard model" of Figure 2). This phenomenon has been noted by many researchers (see Keeley, 1970a). Latour (1970), in a study of A-type stars, proposed that the inversion may result from the crude treatment of convection by the mixing length theory. In the present study it has been noted that the local density maximum occurs at the top of the hydrogen ionization zone (near 7000 K). At this point there is also a rapid change in both the mean molecular weight and the specific heat of the material, a steep temperature gradient, and almost complete cessation of convection. It appears as though a coupling of all of these features with the mixing length theory demands a density inversion in order to satisfy the requirements of hydrostatic and thermal equilibrium.

4. Radiation pressure

In the deeper layers of these models radiation pressure makes a fairly large contribution to the total pressure. This can be seen in Figure 4 where $\beta \equiv P_g/P_{tot}$ has been plotted as a function of mass fraction (M_r/M_*). The maximum contribution of radiation pressure to the total is relatively insensitive to the effective temperature of the model but changes significantly with luminosity. For our "standard" model $\beta_{min} = 0.726$ but

Figure 4. The variation of the gas pressure-to-total pressure ratio (β) as a function of mass fraction

Also included is the total pressure in dyne cm^{-2}.

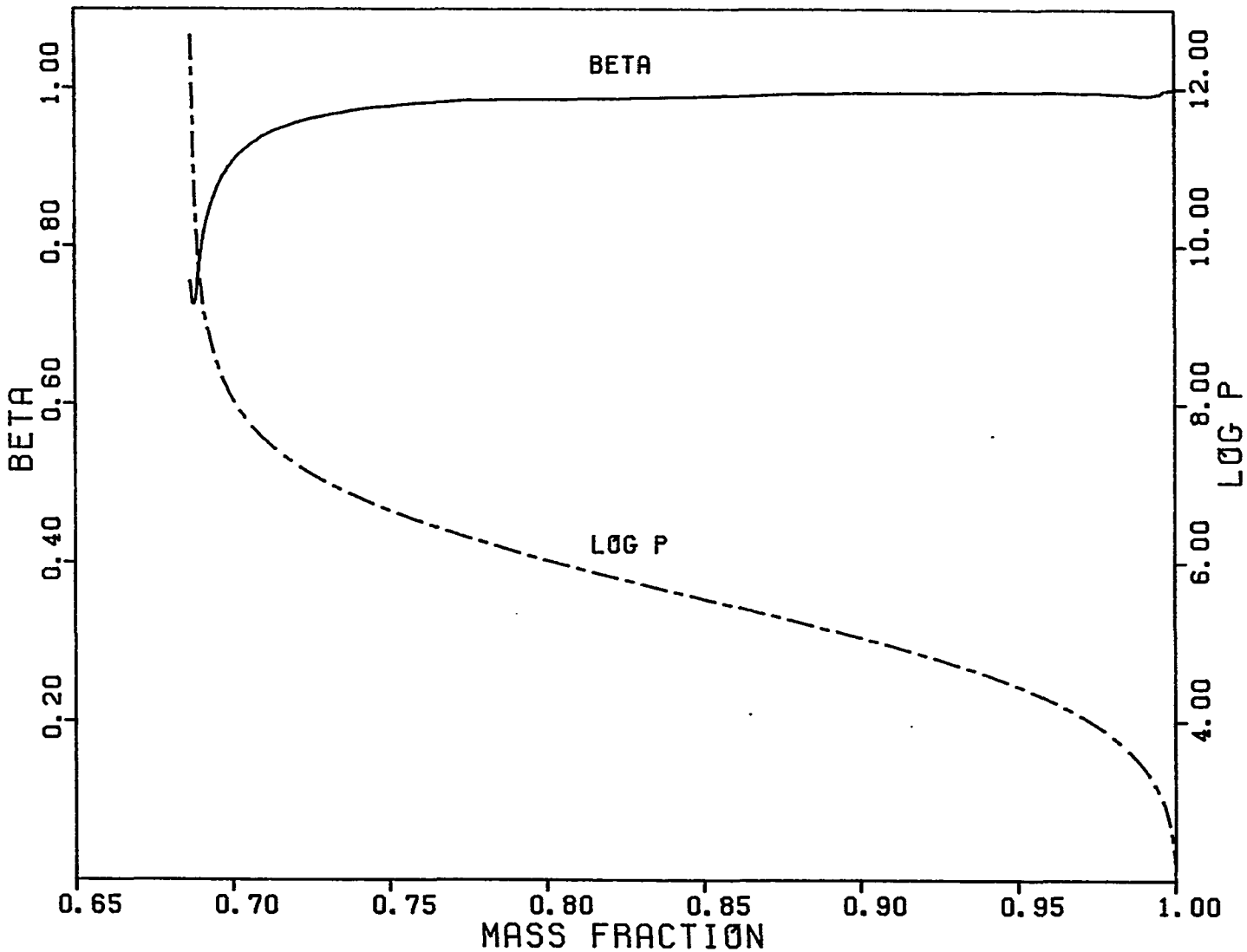
BETA
LOG P
BETA
LOG P
MASS FRACTION
1.00
0.80
0.60
0.40
0.20
12.00
10.00
8.00
6.00
4.00
0.65
0.70
0.75
0.80
0.85
0.90
0.95
1.00

decreases to $\beta_{min} = 0.661$ for a model with $M = 1.0\ M_\odot$, $T_e = 3000$ K, $L = 7000\ L_\odot$, and $\ell/H_p = 2.97$.

The mass fraction location of β_{min} is dependent upon both the total mass of the star and its luminosity. Since the fraction of the stellar mass contained in the core is a function of these parameters (as expressed in the M_c-L relation) and β_{min} is located just above the hydrogen burning shell this result is not unexpected.

5. The ionization and molecular dissociation zones

Other important features of the models in this study are the He^+ and $H - He^o$ ionization zones and the H_2 dissociation zone, the driving regions of stellar pulsations. Because ionization is strongly temperature dependent the He^+ ionization zone is always near $4 \cdot 10^4$K, while both He^o and H ionize in the range $1\text{-}1.5 \cdot 10^4$ K.

The hydrogen and helium ionization zones and the hydrogen molecular dissociation zone are easily recognized by examining either

$$\Gamma_1 \equiv \left.\frac{d \log P}{d \log \rho}\right|_{ad} \tag{3.1}$$

or

$$\Gamma_3 - 1 \equiv \left.\frac{d \log T}{d \log \rho}\right|_{ad} \tag{3.2}$$

where ad refers to adiabatic compression or expansion. If an adiabatic compression is carried out for a gas not undergoing ionization or dissociation, the energy of compression will result in a higher kinetic energy of the particles and a correspondingly higher temperature or pressure.

Because of the increase in T or P with increasing ρ the quantities Γ_1 and Γ_3-1 will be nearly constant over most of the stellar interior. If, on the other hand, the adiabatic compression takes place in a region of partial ionization, the compression energy will go into ionization of the material rather than into kinetic energy of the particles. This will then produce smaller values for Γ_1 and Γ_3-1, allowing identification of the ionizing regions.

Figure 5 shows Γ_3-1 as a function of temperature for our "standard" model. The helium and hydrogen ionization regions are clearly visible as local minima. Also apparent is the existence of a region of molecular dissociation in the outermost layers of the model. Included in Figure 5 is the work function per zone for linear, nonadiabatic, fundamental mode pulsation. Evidently the dominant driving mechanism for this model results from hydrogen ionization, as has been found by other researchers (see Langer, 1969).

The location of the hydrogen ionization zone follows a pattern similar to that found for the location of the top of the convective region. The top of the convection zone is in fact within the region of hydrogen ionization, again pointing to the importance of a realistic treatment of convection in the study of Miras.

6. Turbulent pressure

The inclusion of turbulent pressure does not significantly affect the static structure of red giant model envelopes. The additional contribution to the pressure term does result in slightly less superadiabatic temperature

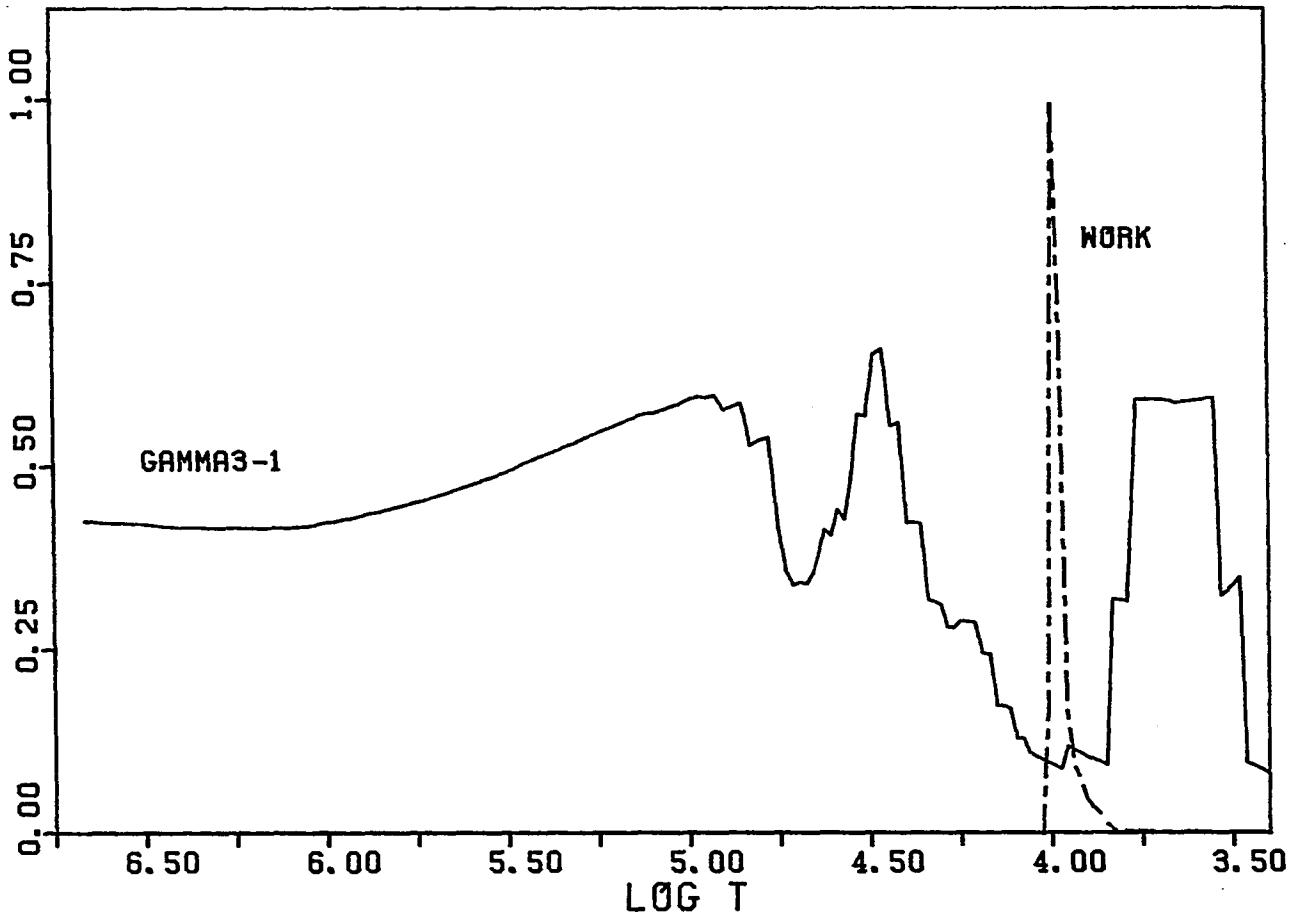

Figure 5. The locations of ionization and fundamental mode pulsational driving regions

The second helium ionization, first helium-hydrogen ionization, and molecular hydrogen dissociation regions are evident by the minima in Γ_3-1 at log T = 4.7, 4.0, and 3.4, respectively. The work function is in arbitrary units.

gradients however, as well as more pronounced density inversions. The values of ℓ/H_p necessary to make the models compatible with the M_c-L relation are also higher.

B. Results of the Linear Pulsation Analysis

1. Adiabatic and nonadiabatic pulsation periods

Results of the linear stability analysis for model envelopes with turbulent pressure neglected are given in Tables 3-6. Given are the adiabatic and nonadiabatic pulsation periods for the fundamental mode and the first and second overtones, as well as Q-values (defined by Equation 1.1), growth rates, and the value of ℓ/H_p required to satisfy both the surface and inner boundary conditions for each model.

For overtone pulsation the adiabatic and nonadiabatic periods differ little (< 10 per cent everywhere), with the adiabatic period always the smaller of the two. For fundamental mode pulsation the periods may be substantially different, with the adiabatic period being almost twice the nonadiabatic value for the lowest mass models having the largest radii (i.e. large luminosities and low effective temperatures). Clearly nonadiabatic effects are most significant in fundamental mode pulsation, becoming increasingly important as the masses of models decrease and their radii increase.

In Figure 6 the nonadiabatic fundamental mode periods have been given for 1.0 $M_\odot$ models showing the dependence of period on location in the H-R diagram. Also included in the diagram are lines of constant radius. As is evident, periods do increase with increasing radius and lines of constant

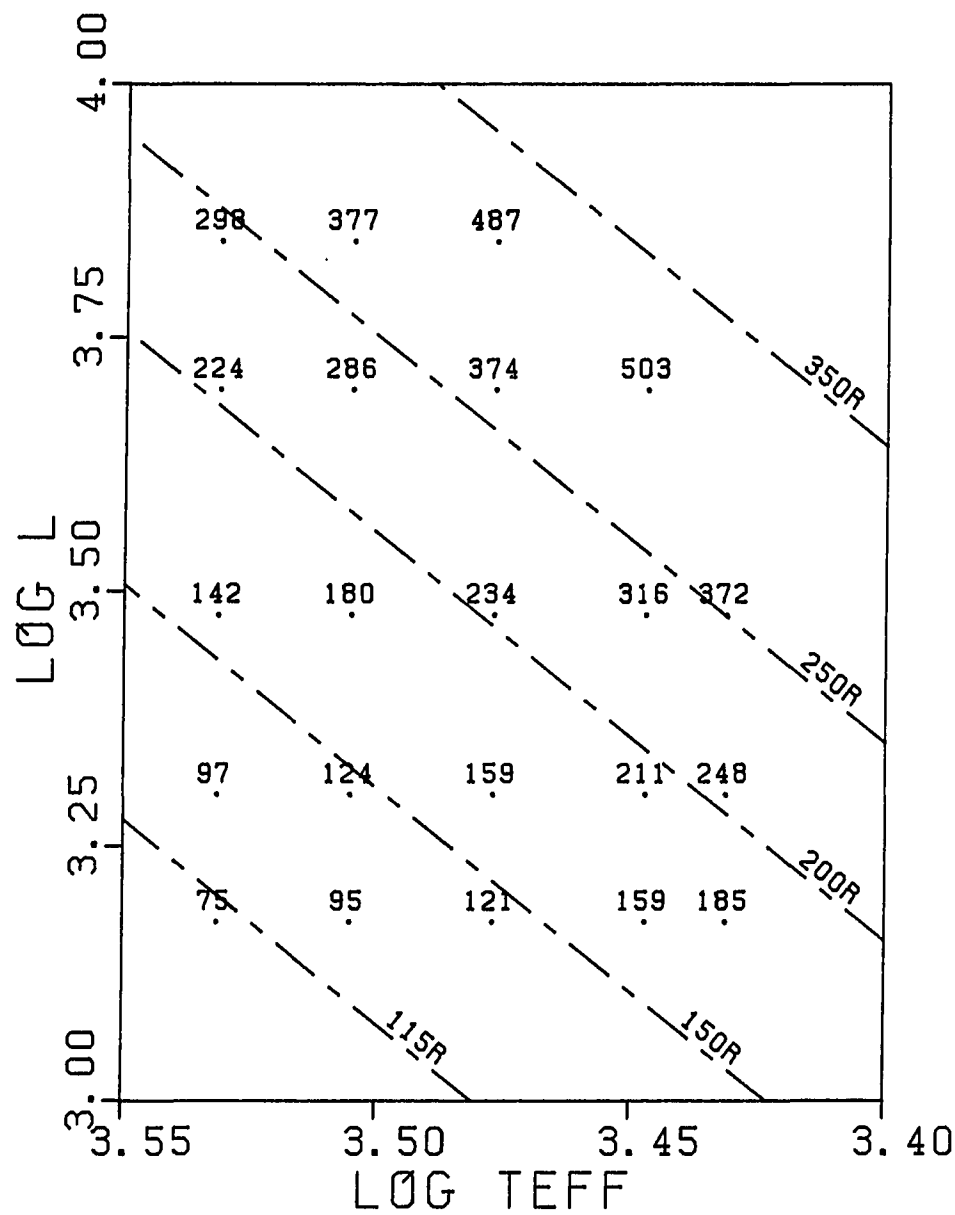

Figure 6. A sample model survey grid in the H-R diagram ($M = 1.0\ M_\odot$)

The fundamental mode periods are given in days. Lines of constant radius have also been included in solar units ($R_\odot = 6.96 \cdot 10^{13}$ cm).

Table 3. Periods, Q-values, and growth rates for 0.8 $M_\odot$ linear models without turbulent pressure

$L/L_\odot$	T_e	ℓ/H_P	P_o^a	P_o	Q_o	η_o
1500	2800	1.61	197.2	197.0	0.0834	0.851
	3000	1.81	148.4	147.9	0.0770	0.704
	3200	2.00	115.2	114.6	0.0724	0.589
	3400	2.22	90.8	90.2	0.0684	0.514
2000	2700	1.66	312.5	307.5	0.0941	1.615
	2800	1.76	267.7	263.4	0.0899	1.437
	3000	1.93	200.1	196.5	0.0825	1.178
	3200	2.25	152.9	150.3	0.0765	1.013
	3400	2.38	122.3	120.0	0.0733	0.914
3000	2700	1.91	497.5	448.9	0.1013	3.142
	2800	2.05	422.3	386.5	0.0973	2.842
	3000	2.27	310.5	287.9	0.0892	2.309
	3200	2.57	233.2	219.1	0.0823	1.939
	3400	2.75	184.0	173.5	0.0782	1.714
5000	2700	2.20	1017.0	667.5	0.1027	5.503
	2800	2.31	821.6	580.0	0.0995	4.993
	3000	2.66	568.6	434.2	0.0917	4.283
	3200	2.91	420.2	338.9	0.0868	3.690
	3400	3.13	322.8	270.5	0.0831	3.194
7000	3000	2.55	1053.1	546.2	0.0896	6.948
	3200	2.92	714.9	439.2	0.0874	6.042
	3400	3.30	508.3	348.1	0.0831	5.096

P_1^a	P_1	Q_1	η_1	P_2^a	P_2	Q_2	η_2
90.8	93.1	0.0394	0.336	57.2	59.6	0.0251	0.094
73.9	75.2	0.0392	0.373	47.1	48.6	0.0253	0.161
60.6	61.3	0.0388	0.396	39.1	40.0	0.0253	0.216
50.2	50.6	0.0384	0.418	32.7	33.3	0.0253	0.263
125.5	130.3	0.0399	0.407	78.2	82.5	0.0253	0.030
112.9	116.6	0.0398	0.486	70.4	73.9	0.0253	0.083
92.1	94.1	0.0395	0.519	57.9	60.1	0.0253	0.184
75.9	77.0	0.0394	0.545	48.2	49.6	0.0253	0.241
62.7	63.4	0.0387	0.580	40.0	40.9	0.0250	0.297
169.3	178.2	0.0402	0.589	104.9	111.9	0.0253	-0.023
153.1	160.2	0.0403	0.644	94.1	99.9	0.0252	0.018
125.1	129.2	0.0400	0.770	77.3	81.1	0.0251	0.145
103.3	105.8	0.0397	0.832	64.4	66.9	0.0251	0.239
85.6	87.0	0.0392	0.892	53.6	55.3	0.0249	0.324
244.9	265.4	0.0408	0.726	153.2	165.9	0.0255	-0.105
221.4	238.1	0.0409	0.857	136.1	147.3	0.0253	-0.110
182.3	192.4	0.0406	1.109	110.3	117.0	0.0247	-0.045
151.7	157.9	0.0405	1.274	91.8	96.3	0.0247	0.109
127.0	130.6	0.0401	1.371	77.5	80.4	0.0247	0.258
227.8	239.7	0.0390	1.299	136.4	146.6	0.0240	-0.235
191.4	200.8	0.0400	1.439	112.7	117.8	0.0234	-0.143
161.5	168.6	0.0402	1.578	95.3	98.2	0.0234	0.021

Table 4. Periods, Q-values, and growth rates for 1.0 $M_\odot$ linear models without turbulent pressure

$L/L_\odot$	T_e	ℓ/H_P	P_o^a	P_o	Q_o	η_o
1500	2700	1.40	184.4	185.3	0.0787	0.436
	2800	1.50	158.8	159.4	0.0755	0.389
	3000	1.71	121.0	121.2	0.0706	0.339
	3200	1.87	94.6	94.6	0.0669	0.270
	3400	2.07	75.0	74.9	0.0635	0.229
2000	2700	1.53	248.0	248.3	0.0850	0.767
	2800	1.68	210.7	210.8	0.0805	0.688
	3000	1.90	159.1	158.8	0.0746	0.558
	3200	2.09	124.0	123.6	0.0704	0.467
	3400	2.22	97.7	97.3	0.0665	0.387
3000	2700	1.79	381.6	372.2	0.0940	1.736
	2800	1.91	322.2	315.7	0.0889	1.423
	3000	2.21	239.5	234.4	0.0812	1.176
	3200	2.47	183.4	179.7	0.0755	1.004
	3400	2.61	144.7	142.0	0.0716	0.855
5000	2800	2.27	572.1	502.8	0.0965	3.042
	3000	2.61	414.4	373.8	0.0883	2.546
	3200	2.93	311.5	285.7	0.0819	2.154
	3400	3.21	241.8	224.3	0.0771	1.863
7000	3000	2.97	613.3	487.1	0.0894	3.843
	3200	3.24	453.7	377.0	0.0839	3.235
	3400	3.50	348.8	298.1	0.0796	2.806

p_1^a	p_1	Q_1	η_1	p_2^a	p_2	Q_2	η_2
91.7	93.6	0.0397	0.220	58.4	60.4	0.0256	0.066
82.1	83.5	0.0395	0.233	52.7	54.3	0.0257	0.096
66.4	67.2	0.0392	0.259	43.1	44.0	0.0256	0.141
54.1	54.5	0.0386	0.268	35.5	36.2	0.0256	0.186
44.9	45.2	0.0383	0.273	29.8	30.2	0.0254	0.208
113.4	116.4	0.0398	0.307	71.4	74.4	0.0255	0.074
102.5	104.8	0.0400	0.325	65.0	67.4	0.0257	0.108
83.1	84.4	0.0396	0.356	53.5	55.0	0.0258	0.170
68.1	68.7	0.0392	0.380	44.4	45.3	0.0258	0.232
56.6	57.0	0.0389	0.385	37.2	37.8	0.0258	0.264
153.6	159.3	0.0402	0.470	95.2	100.5	0.0254	0.048
139.6	143.7	0.0405	0.510	87.3	91.4	0.0257	0.113
113.9	116.2	0.0402	0.580	71.9	74.6	0.0258	0.215
93.7	95.1	0.0400	0.609	59.8	61.5	0.0258	0.281
77.3	78.0	0.0393	0.619	49.8	50.9	0.0257	0.333
206.3	216.2	0.0415	0.843	126.8	135.1	0.0259	0.034
167.7	173.5	0.0410	0.956	103.4	108.6	0.0256	0.155
138.4	141.8	0.0406	1.031	86.3	89.7	0.0257	0.265
115.1	117.0	0.0402	1.072	72.4	74.8	0.0257	0.359
215.3	226.7	0.0416	1.173	131.0	139.0	0.0255	-0.006
179.2	185.9	0.0414	1.367	109.4	114.4	0.0255	0.162
148.8	152.5	0.0407	1.412	91.8	95.1	0.0254	0.280

Table 5. Periods, Q-values, and growth rates for 1.4 $M_\odot$ linear models without turbulent pressure

$L/L_\odot$	T_e	ℓ/H_P	P_o^a	P_o	Q_o	η_o
1500	2700	1.22	140.9	141.4	0.0710	0.134
	2800	1.24	122.5	122.8	0.0688	0.116
	3000	1.42	94.1	94.2	0.0649	0.096
	3200	1.65	74.0	74.0	0.0619	0.080
	3400	1.85	59.3	59.3	0.0595	0.062
2000	2700	1.36	185.2	185.9	0.0753	0.252
	2800	1.45	159.9	160.3	0.0724	0.226
	3000	1.57	122.3	122.4	0.0680	0.174
	3200	1.84	95.7	95.7	0.0645	0.149
	3400	2.02	76.6	76.5	0.0619	0.117
3000	2700	1.53	275.8	276.1	0.0825	0.552
	2800	1.69	236.8	236.8	0.0789	0.500
	3000	1.84	179.6	179.1	0.0734	0.389
	3200	2.10	139.3	138.8	0.0690	0.338
	3400	2.24	110.4	110.1	0.0657	0.266
5000	2700	1.93	470.2	457.7	0.0932	1.487
	2800	1.97	400.3	390.0	0.0886	1.286
	3000	2.31	297.3	290.7	0.0812	1.046
	3200	2.46	227.8	223.4	0.0757	0.850
	3400	2.71	178.4	175.4	0.0713	0.694
7000	2800	2.36	576.6	533.0	0.0940	2.232
	3000	2.65	422.4	396.0	0.0860	1.842
	3200	2.92	318.8	302.7	0.0797	1.476
	3400	3.13	248.8	237.8	0.0751	1.241

P_1^a	P_1	Q_1	η_1	P_2^a	P_2	Q_2	η_2
78.2	79.1	0.0397	0.124	50.4	51.5	0.0259	0.055
69.9	70.6	0.0396	0.129	45.3	46.2	0.0259	0.072
56.0	56.4	0.0389	0.140	36.8	37.4	0.0258	0.104
45.6	45.8	0.0383	0.145	30.3	30.7	0.0257	0.121
37.4	37.5	0.0376	0.148	25.3	25.5	0.0256	0.137
97.4	98.8	0.0400	0.182	62.1	63.8	0.0258	0.074
87.8	88.9	0.0401	0.191	56.3	57.6	0.0260	0.095
70.6	71.3	0.0396	0.205	46.0	46.8	0.0260	0.142
57.5	57.9	0.0390	0.213	37.9	38.4	0.0259	0.162
47.2	47.4	0.0383	0.213	31.5	31.8	0.0257	0.189
133.7	136.4	0.0407	0.303	84.2	87.2	0.0260	0.112
120.2	122.3	0.0407	0.319	76.2	78.6	0.0262	0.140
97.5	98.5	0.0404	0.347	62.6	64.1	0.0263	0.212
79.4	79.9	0.0397	0.365	51.5	52.4	0.0261	0.258
65.7	65.9	0.0393	0.357	43.1	43.6	0.0260	0.274
198.5	204.2	0.0416	0.551	123.0	129.1	0.0263	0.129
178.5	182.6	0.0415	0.597	111.0	115.9	0.0263	0.196
145.2	147.4	0.0412	0.634	91.4	94.4	0.0264	0.279
118.9	120.1	0.0407	0.653	75.6	77.6	0.0263	0.342
98.5	98.9	0.0402	0.663	63.4	64.7	0.0263	0.400
231.0	283.5	0.0421	0.829	142.1	150.1	0.0265	0.150
188.1	192.1	0.0417	0.905	116.8	121.7	0.0264	0.271
153.9	156.1	0.0411	0.954	96.8	100.1	0.0264	0.361
128.2	129.1	0.0408	0.969	81.3	83.6	0.0263	0.454

Table 6. Periods, Q-values, and growth rates for 2.0 $M_\odot$ linear models without turbulent pressure

$L/L_\odot$	T_e	ℓ/H_P	P_o^a	P_o	Q_o	η_o
1500	2700	1.00	112.7	112.8	0.0677	0.036
	2800	1.09	98.1	98.2	0.0657	0.033
	3000	1.22	76.6	76.6	0.0631	0.023
	3200	1.42	60.5	60.5	0.0605	0.019
	3400	1.60	48.9	48.9	0.0586	0.016
2000	2700	1.11	146.5	146.7	0.0710	0.068
	2800	1.22	125.9	126.0	0.0680	0.063
	3000	1.38	96.8	96.9	0.0643	0.053
	3200	1.52	76.9	76.9	0.0620	0.039
	3400	1.69	62.4	62.4	0.0603	0.027
3000	2700	1.27	215.1	215.5	0.0770	0.157
	2800	1.41	184.9	185.1	0.0737	0.142
	3000	1.60	140.4	140.5	0.0688	0.117
	3200	1.81	109.7	109.7	0.0652	0.095
	3400	1.98	87.6	87.6	0.0624	0.077
5000	2700	1.61	349.5	349.0	0.0850	0.502
	2800	1.71	301.4	300.8	0.0817	0.417
	3000	1.95	226.0	225.5	0.0753	0.345
	3200	2.17	175.6	175.0	0.0709	0.264
	3400	2.29	139.5	139.1	0.0676	0.209
7000	2700	1.85	491.3	485.0	0.0917	0.999
	2800	1.98	420.5	415.3	0.0876	0.853
	3000	2.22	312.5	308.5	0.0800	0.689
	3200	2.46	240.4	237.8	0.0749	0.537
	3400	2.68	189.5	187.8	0.0709	0.420

P_1^a	P_1	Q_1	η_1	P_2^a	P_2	Q_2	η_2
64.5	64.9	0.0390	0.065	42.1	42.7	0.0256	0.037
57.2	57.5	0.0385	0.066	37.7	38.2	0.0256	0.043
45.6	45.8	0.0378	0.066	30.8	31.1	0.0256	0.058
36.8	39.9	0.0369	0.069	25.4	25.6	0.0255	0.068
29.9	30.0	0.0359	0.073	21.0	21.1	0.0254	0.083
81.2	81.9	0.0396	0.096	52.3	53.1	0.0257	0.055
72.2	72.7	0.0392	0.107	46.9	47.6	0.0257	0.065
57.2	57.6	0.0382	0.109	37.9	38.3	0.0254	0.085
46.2	46.3	0.0373	0.102	31.1	31.4	0.0253	0.095
38.1	38.2	0.0369	0.097	26.2	26.4	0.0255	0.100
113.9	115.2	0.0411	0.170	72.1	73.7	0.0263	0.095
101.0	102.0	0.0406	0.177	64.5	65.7	0.0262	0.111
80.7	81.3	0.0398	0.186	52.3	53.1	0.0260	0.139
65.2	65.6	0.0390	0.190	43.0	43.5	0.0258	0.158
52.9	53.1	0.0379	0.187	35.4	35.7	0.0255	0.172
169.0	171.7	0.0418	0.332	105.1	108.4	0.0264	0.150
151.1	153.2	0.0416	0.341	94.9	97.5	0.0265	0.184
121.6	122.8	0.0410	0.362	77.1	78.8	0.0263	0.226
99.0	99.5	0.0403	0.366	63.7	64.7	0.0262	0.273
81.2	81.4	0.0395	0.362	53.0	53.6	0.0260	0.300
218.4	223.2	0.0423	0.488	134.7	140.2	0.0265	0.167
197.4	200.8	0.0423	0.517	122.4	126.6	0.0267	0.222
159.0	160.5	0.0417	0.559	99.5	102.1	0.0265	0.305
129.7	130.4	0.0411	0.563	82.2	83.9	0.0264	0.354
106.3	106.6	0.0402	0.553	68.5	69.6	0.0263	0.396

period and radius roughly correspond. The fact that lines of constant period and radius do not exactly agree implies that Q (the pulsation "constant") is a slowly varying function of the stellar parameters. Examination of Tables 3-6 shows that Q_o obtains a maximum value of 0.1027 in this survey for the 0.8 $M_\odot$ model with L = 5000 $L_\odot$ and T_e = 2700 K and a minimum value of 0.0586 for the 2.0 $M_\odot$ model with L = 1500 $L_\odot$ and T_e = 3400 K.

2. Characteristics of the eigenvectors

The radial, adiabatic eigenvectors associated with our "standard" model are shown in Figure 7. Because of the conservative nature of adiabatic oscillations (i.e. no net energy gains or losses within a zone) the stellar structure passes through its equilibrium configuration twice each period with 0, 1, and 2 nodes for fundamental mode (F), first overtone (1H), and second overtone (2H) pulsation, respectively. The node for first overtone pulsation has been found to occur just below the zone of dominant driving at $M_r/M_* = 0.99$ while for this model the second overtone has one node on either side of the driving region. It is also apparent that the largest motions occur in the outermost layers of the envelope for all nodes.

For nonadiabatic pulsation the oscillations are no longer conservative and the structure never strictly passes through its equilibrium configuration. The radial eigenvectors have been plotted in Figures 8-10 for our "standard" model for fundamental mode, first overtone, and second overtone pulsation, respectively. Apparently no true nodes exist where

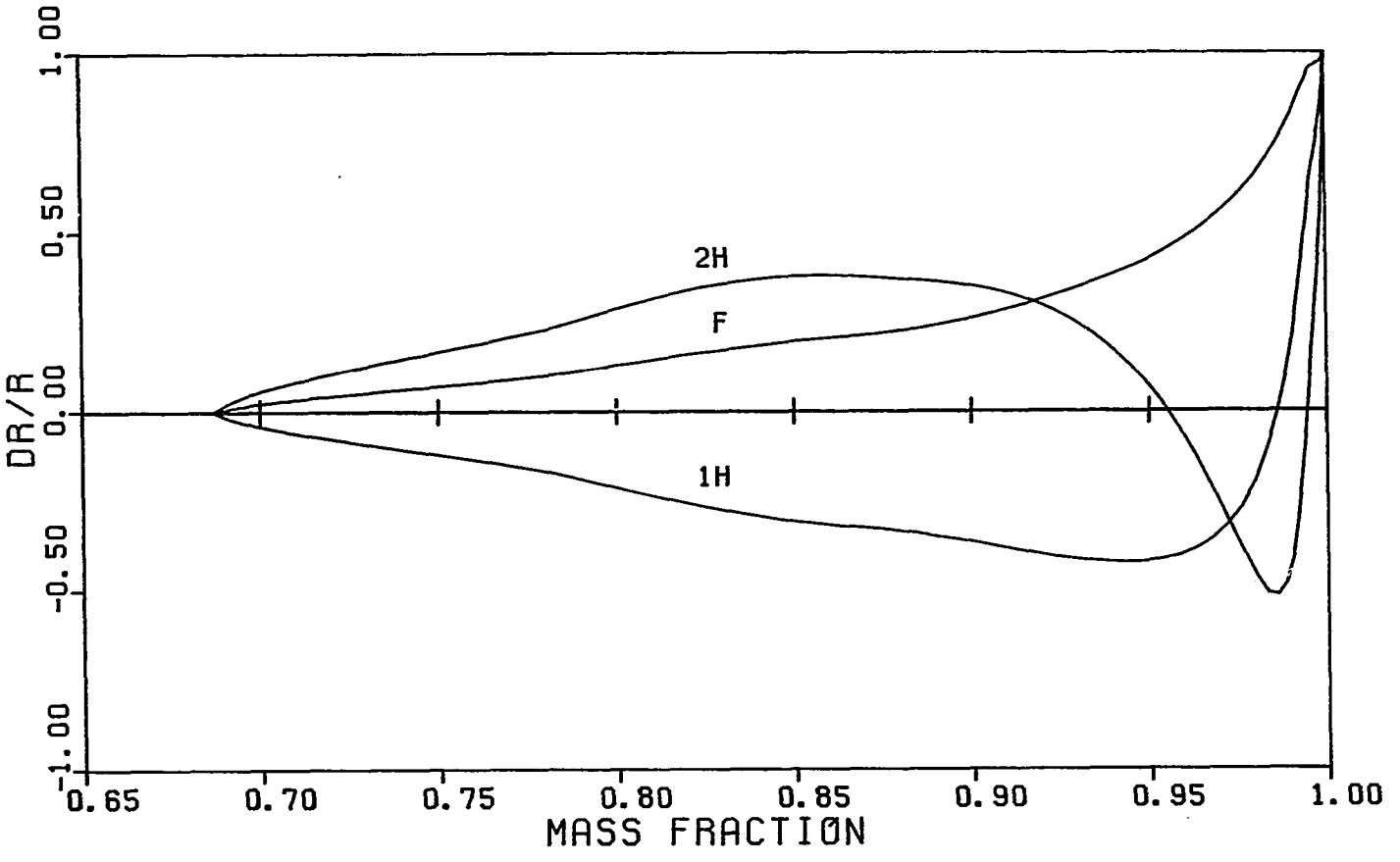

Figure 7. Radial eigenvectors for linear, adiabatic pulsation

The fundamental mode, first overtone, and second overtone are labelled F, 1H, and 2H, respectively. The nodes for the first and second overtones occur at 10,200 K and at 14,200 K and 7700 K, respectively while maximum driving occurs at 9800 K. All radial eigenvectors have been normalized to unity at the surface.

motion is always zero; instead, running waves are present in the envelope as evidenced by the phase of the eigenvectors as a function of mass fraction (see Equations 2.15).

During nonadiabatic pulsation, variations in structure parameters are not expected to occur in phase. For each mode the differences in phase of the various eigenvectors at any particular level may be seen as demonstrated by Figures 8, 11, and 12 where the radial, density, and pressure eigenvectors, respectively, have been plotted as a function of mass fraction for fundamental mode pulsation. At $M_r/M_* = 0.987$, corresponding to a hydrostatic temperature of T = 9829 K and the zone of strongest driving (see Figure 5), the pressure maximum occurs after peak compression, just as expected. After maximum density has been obtained in the zone and expansion has begun, the pressure in that zone reaches a maximum, driving the expansion further. The local maxima seen in the amplitudes of the radial and density variations also correspond to the driving region (local maxima also occur for the temperature and radiative luminosity eigenvectors).

3. Growth rates and nonadiabaticity

The nonadiabatic pulsation analysis reveals that very large linear growth rates exist for many models, particularly for the fundamental mode. Values of η_o of several hundred per cent per period are not uncommon for the less massive models. Apparently, the driving that exists in the zones of partial hydrogen ionization overwhelms the damping that exists throughout most of the rest of the star. In cases where the growth rates are smaller the effects of damping are more apparent and may even quench

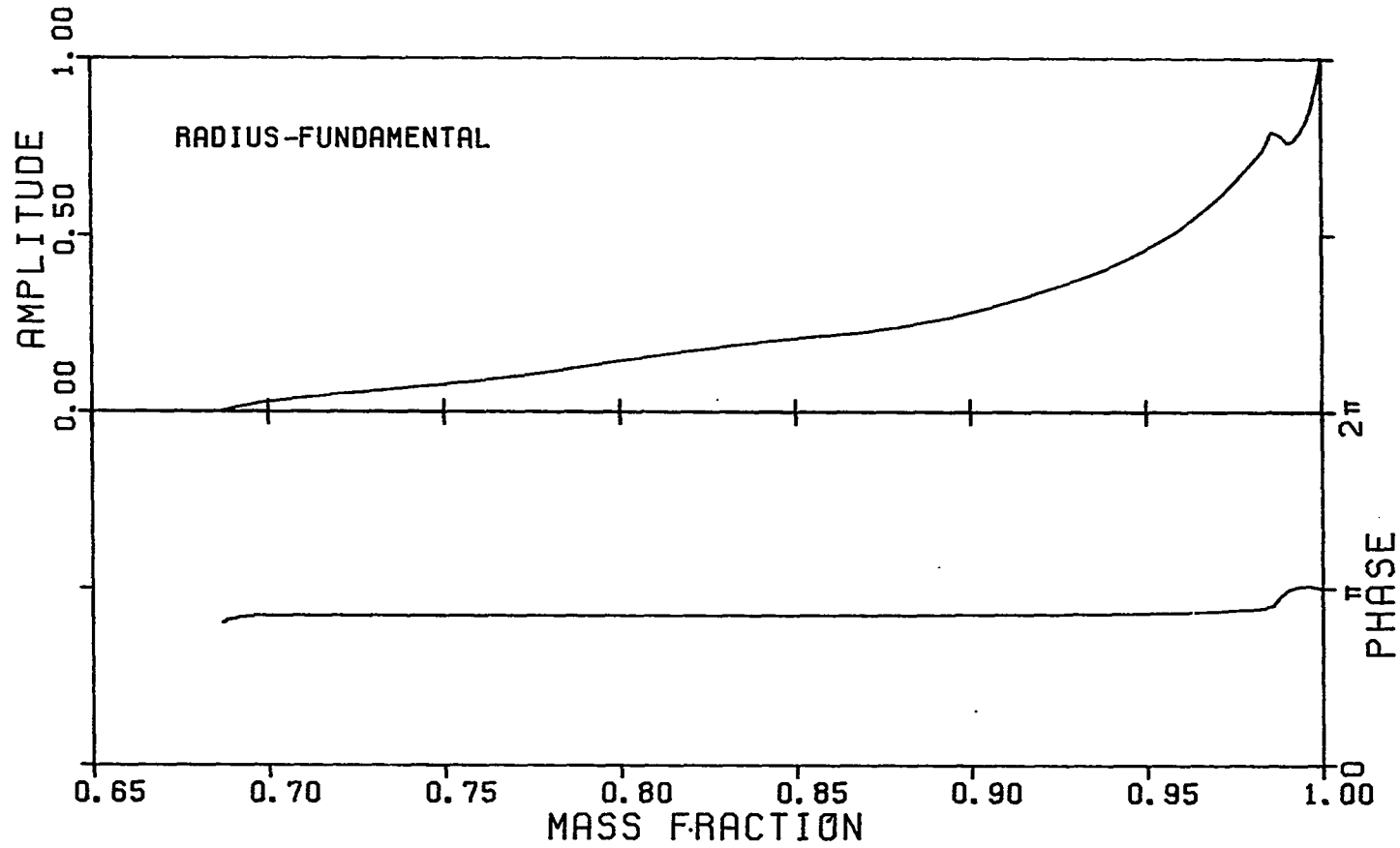

Figure 8. The radial, nonadiabatic, fundamental mode eigenvector

The eigenvector displays a local amplitude maximum in the region of maximum driving. The phase has been normalized to π at the surface.

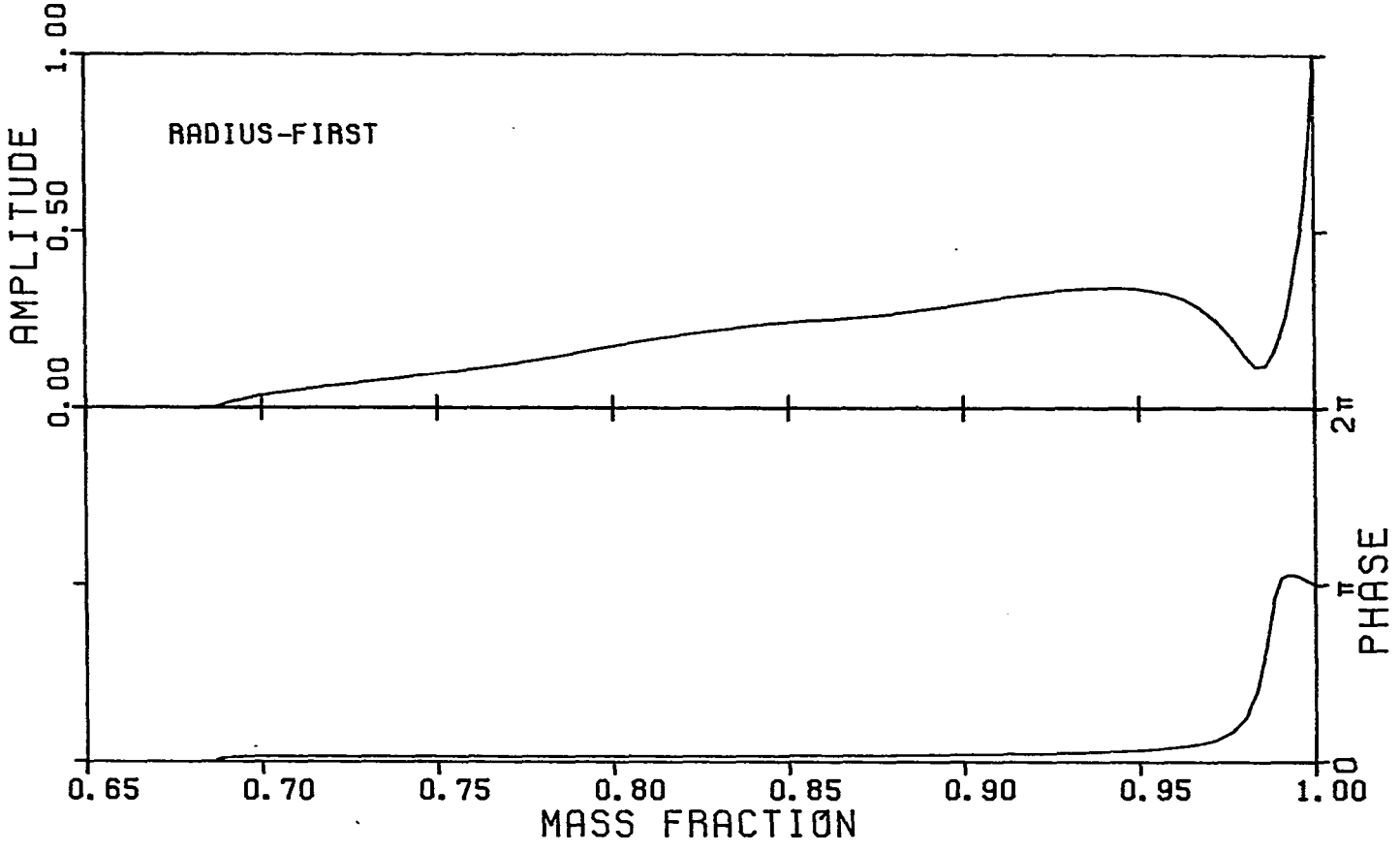

Figure 9. The radial, nonadiabatic, first overtone eigenvector

The eigenvector has an amplitude minimum at the node position for the corresponding adiabatic eigenvector. A phase shift of 180° occurs at the node.

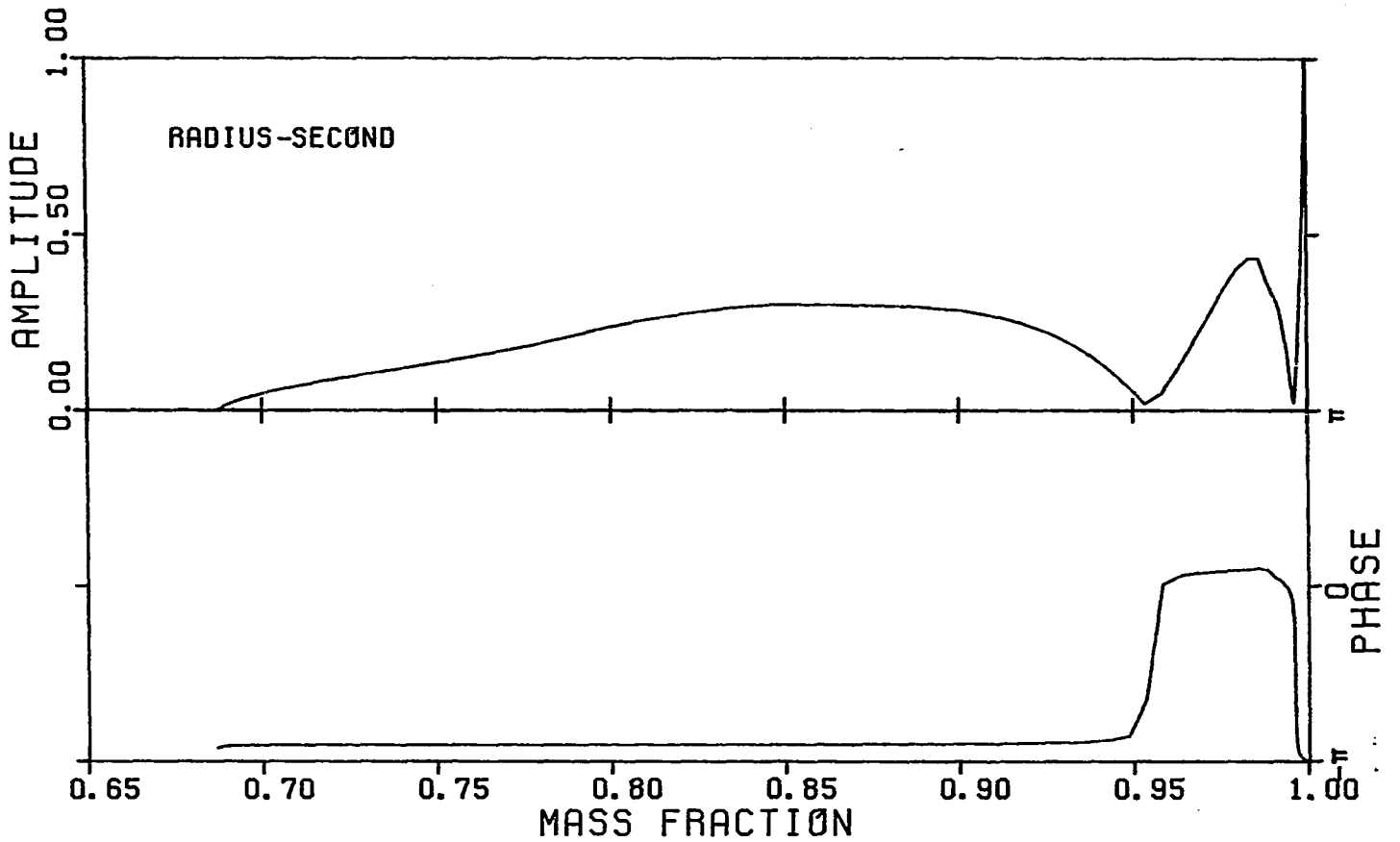

Figure 10. The radial, nonadiabatic, second overtone eigenvector

The eigenvector shows phase shifts of 180° at each node. The nodes correspond to those of the adiabatic eigenvector

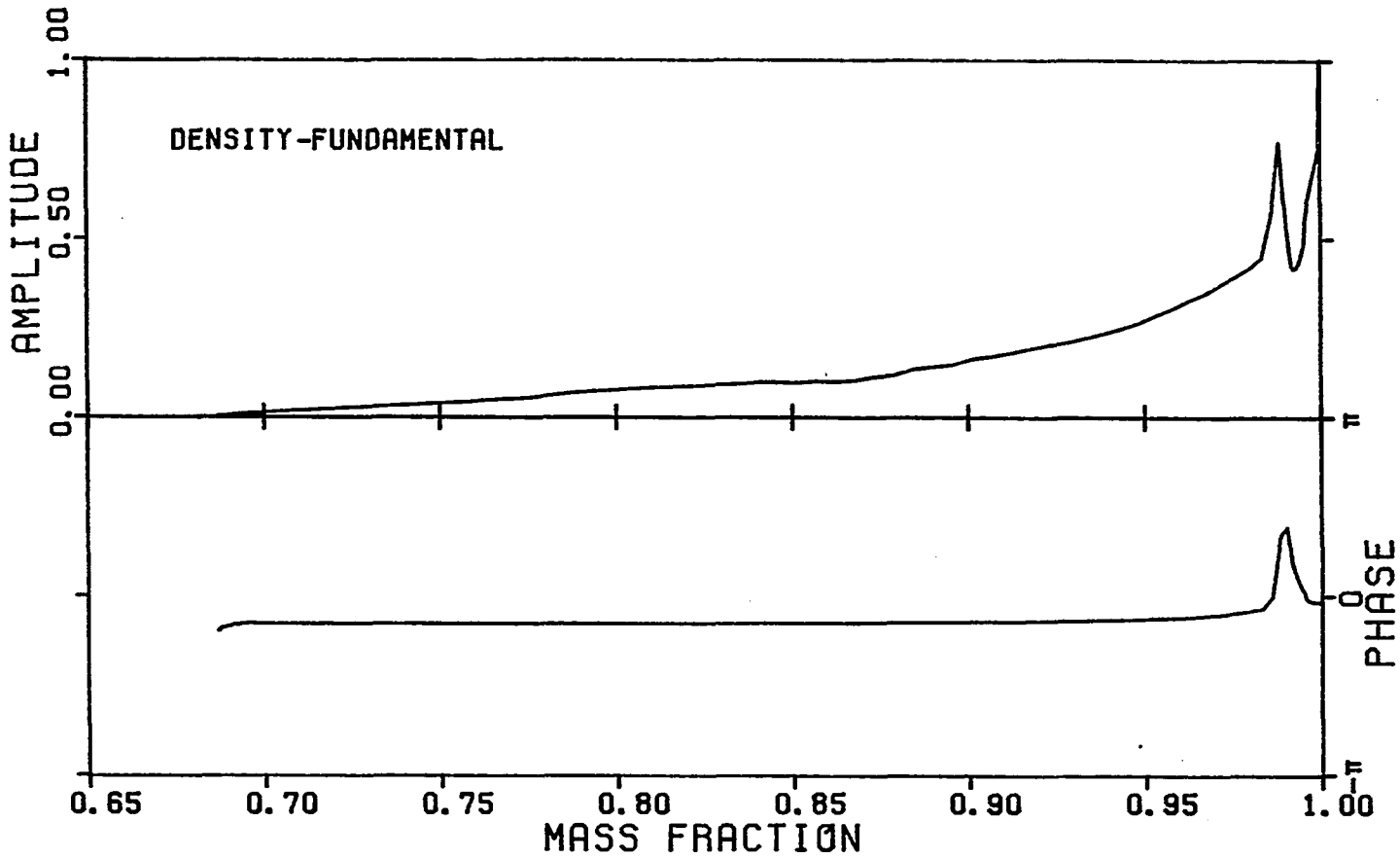

Figure 11. The density variations for nonadiabatic fundamental mode pulsation

A local amplitude maximum and the corresponding abrupt phase shift coincide with the driving region. The amplitude has been artificially normalized to unity here, actually $|\delta\rho/\rho|_{max} / |\delta r/r|_{max} = 8.146$.

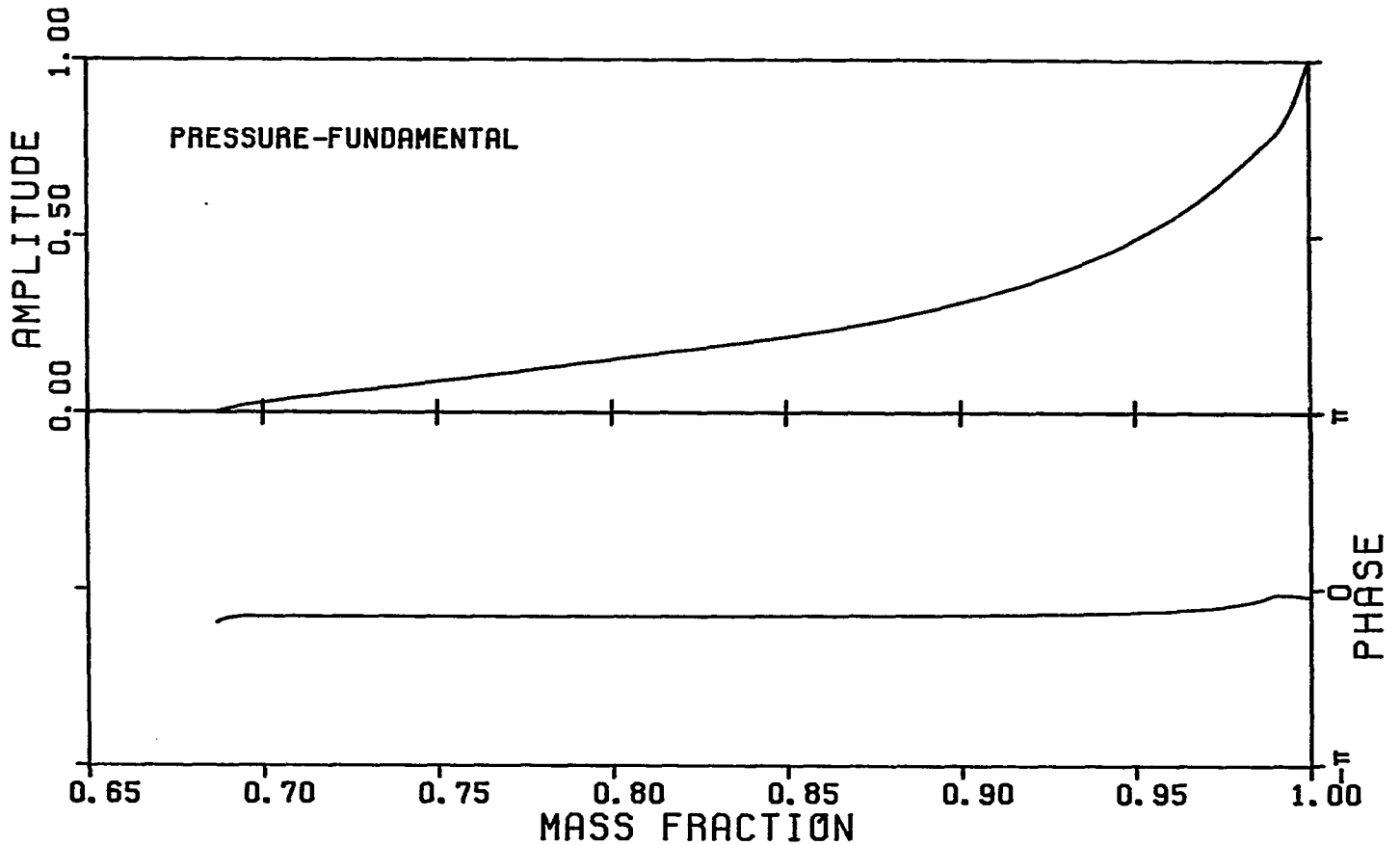

Figure 12. The pressure variations for nonadiabatic, fundamental mode pulsation

Effects of driving on the eigenvector are only weakly apparent. $|\delta P/P|_{max}/|\delta r/r|_{max}=5.739$.

pulsation, as occurs when $\eta_1 < 0$. In such situations the amount of driving that exists in the ionization regions is insufficient to overcome damping. Only second overtone oscillations were ever found to be pulsationally stable (i.e. with $\eta < 0$) and then only for a small number of models.

It is the presence of nonadiabatic effects that governs the growth or decay of stellar pulsations, and the degree to which oscillations are nonadiabatic has been found to be well-correlated with the linear growth rates of the fundamental mode. Inspection of Tables 3-6 shows that η_0 tends to be larger for models of lower mass and larger radius. Qualitatively this results because heat exchange may be more rapid in a low density material.

The amount of nonadiabaticity in stellar pulsations may be estimated by comparing the thermal (or Kelvin) time scale to the pulsation period. If the Kelvin time is of the same order as the pulsation period, adiabaticity becomes a poor assumption. The Kelvin time (Cox, 1980) may be estimated by considering the ratio of the total internal (thermal) energy content of a star to its luminosity,

$$t_K \sim E_{th}/L. \tag{3.3}$$

The amount of thermal energy may be related to the star's gravitational energy through use of the virial theorem yielding the expression

$$t_K \sim \frac{3}{4}\frac{GM^2}{LR} \tag{3.4a}$$

$$\sim 2\cdot 10^7 \frac{M^2}{LR} \text{ years} \tag{3.4b}$$

where M, L, and R are all in solar units. Finally, if Equation 1.1 for the pulsation period is used, the ratio of the Kelvin time to the period of a star may be written

$$\frac{t_K}{P_i} \sim 7 \cdot 10^9 \frac{1}{Q_i} \cdot \frac{M^{5/2}}{R^{5/2} L} . \tag{3.5}$$

where Q is in days. Since Q_i is only slowly varying for a given mode it is apparent that the amount of nonadiabaticity is a strong function of both the mass and the radius, as expected.

For a Mira with $M = 2.0\ M_\odot$, $L = 2000\ L_\odot$, and $R = 200\ R_\odot$ we have $t_K \sim 200$ years, much longer than any observed period ($\frac{t_K}{P_o} \sim 530$). However, for a Mira with $M = 0.8\ M_\odot$, $L = 7000\ L_\odot$, and $R = 300\ R_\odot$, the Kelvin time is $t_K \sim 6$ years, compared with a fundamental mode period of approximately 1.6 years ($\frac{t_K}{P_o} \sim 3.8$). Clearly in the latter case nonadiabatic effects will be pronounced. When overtone pulsation is considered, nonadiabatic effects will certainly be less severe because of the much shorter periods ($\frac{P_1}{P_o} = \frac{Q_1}{Q_o} \sim 0.5$).

Figure 13 demonstrates the dependence of fundamental mode growth rates on the degree of nonadiabaticity. For models having a Kelvin time much larger than the pulsation period, oscillations are nearly adiabatic and the resulting growth rates are small. If the Kelvin time is near the fundamental mode period, growth rates may be quite large. The effects of large growth rates and extreme nonadiabaticity are of crucial importance in the full amplitude calculations to be discussed later.

Figure 13. The effects of nonadiabaticity on fundamental mode growth rates for models with turbulent pressure neglected

The growth rate is seen to be a strong function of the Kelvin time-to-pulsation period ratio (t_k/P).

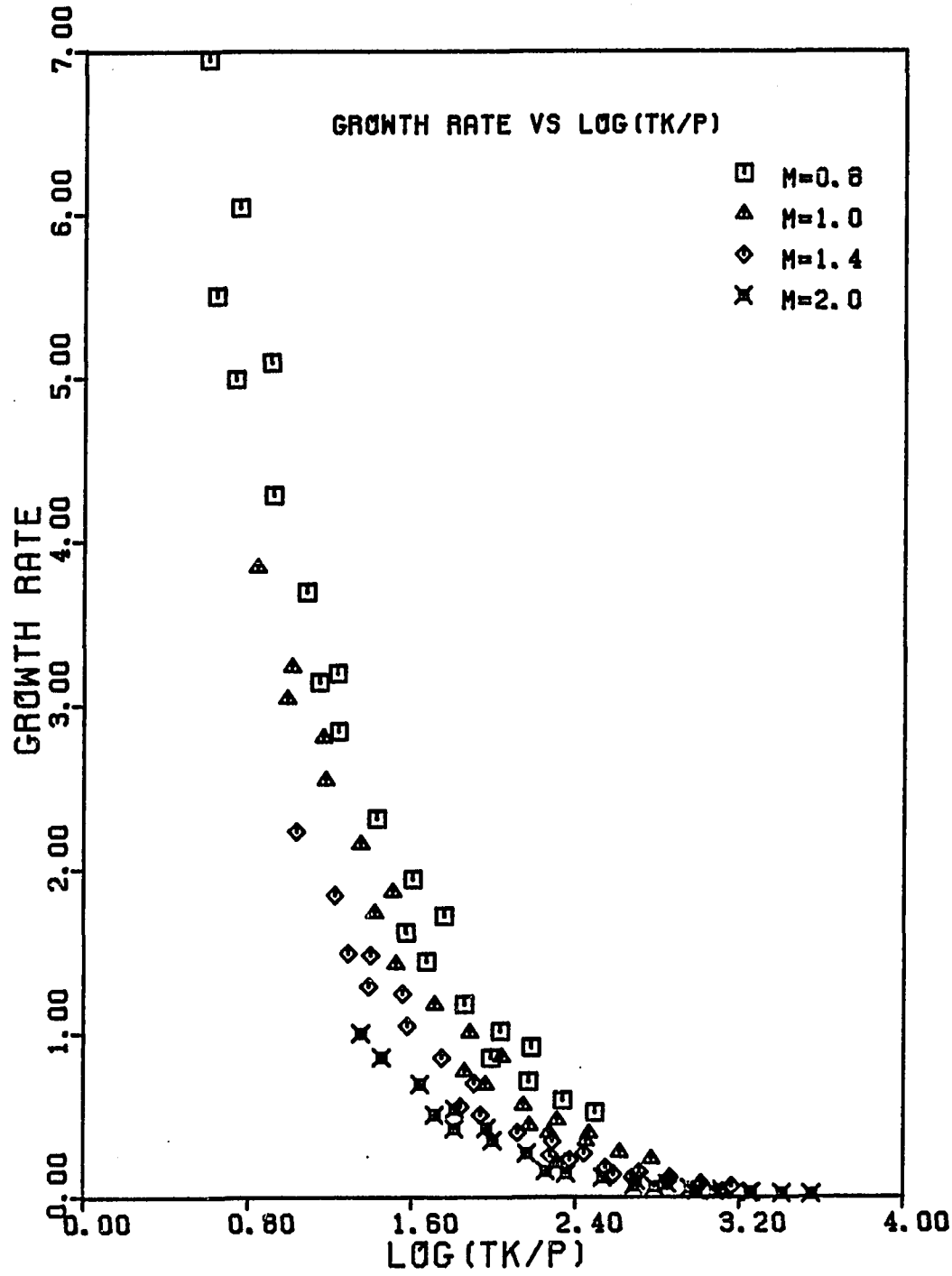
GROWTH RATE VS LOG(TK/P)
M=0.6
M=1.0
M=1.4
M=2.0
GROWTH RATE
LOG(TK/P)
0.00
1.00
2.00
3.00
4.00
5.00
6.00
7.00
0.00
0.80
1.60
2.40
3.20
4.00

4. Effects of turbulent pressure

The inclusion of turbulent pressure in pulsation models apparently leads to more severe nonadiabaticity as is evident from the periods and growth rates given in Table 7. These models were used in the nonlinear calculations to be discussed in the next chapter but were also investigated by the linear techniques already described. Models 1 and 2 differ only in the absence or presence of turbulent pressure but the resulting periods have changed appreciably. The adiabatic fundamental mode period increased by more than a factor of two when turbulent pressure was included while the nonadiabatic period increased by about 25 per cent. The linear growth rate for fundamental mode pulsation also increased significantly (69 per cent).

The other models of Table 7 may be compared to their counterparts of Tables 3-6. As expected from the analysis of the last section, the amount by which the adiabatic and nonadiabatic fundamental mode periods differ, and the magnitude of the linear, fundamental mode growth rates depend upon the mass, radius, and luminosity of the models, with the less massive models of larger radius and greater luminosity being least adiabatic. Presumably the enhanced nonadiabaticity of the turbulent pressure models results from the need for less material to support the overlying layers with the result that the lower density allows for more rapid thermal adjustment between adjacent zones. This simple picture is complicated somewhat however, by the higher values of ℓ/H_p needed in the turbulent pressure models to increase the density sufficiently to meet the surface and inner boundary conditions. With the larger values of

Table 7. Initial DYNSTAR models - linear analysis

Model	$M/M_\odot$	$L/L_\odot$	T_e	ℓ/H_P	P_o^a	P_o	Q_o	η_o
1	0.8	5000	3275	2.66	394.0	339.8	0.0933	3.823
2	0.8	5000	3275	2.88	898.8	422.9	0.1161	6.454
3	0.8	5000	3000	2.53	2616.6	591.1	0.1248	7.400
4	1.4	5000	3000	2.00	332.6	328.6	0.0918	1.322
5	1.4	3000	3000	1.52	193.7	194.3	0.0796	0.388
6	1.4	3000	2700	1.30	298.6	301.2	0.0900	0.534

P_1^a	P_1	Q_1	η_1	P_2^a	P_2	Q_2	η_2	P_{turb}
142.3	148.9	0.0409	0.610	83.9	91.0	0.0250	-0.132	no
159.0	164.9	0.0453	0.662	89.1	95.8	0.0263	-0.163	yes
203.0	214.1	0.0452	0.530	115.5	132.0	0.0279	-0.231	yes
150.9	154.9	0.0433	0.401	93.6	97.7	0.0273	0.078	yes
100.4	101.9	0.0418	0.218	63.2	64.8	0.0265	0.090	yes
137.6	141.2	0.0422	0.194	85.4	89.4	0.0267	0.035	yes

ℓ/H_P a convective element is able to traverse an increased number of pressure scale heights, allowing thermal information to be transported further and enhancing the nonadiabaticity.

C. Comparison with Observations - The PMR Relations

Results of the linear, nonadiabatic pulsation analysis may be compared with observations through period-mass-radius (PMR) relations, of which Equation 1.1 defining the pulsation "constant" is an example. To find the dependence of period (or equivalently, Q) on mass and radius, a least squares fit of the results given in Tables 3-6 for the models with turbulent pressure neglected has been used. For fundamental mode pulsation

$$\log P_o = -1.92 - 0.73 \log M + 1.86 \log R \tag{3.6}$$

and for first overtone pulsation

$$\log P_1 = -1.60 - 0.51 \log M + 1.59 \log R \tag{3.7}$$

where periods are given in days and the mass and radius are in solar units. These PMR relations provide a means for rapid interpolation between models calculated here and may also be used (with caution) to extrapolate to masses and radii not considered in this study should the current estimates for these stellar parameters be modified.

In a recent paper, Fox and Wood (1982) have also derived a PMR relation for fundamental mode pulsation from their survey of linear, nonadiabatic variable star models along the AGB. For stars with $0.8 < M/M_\odot < 3.0$

they find $P_o = Q_o^1 M^{-0.8} R^2$, where $Q_o^1 = 6.1 \cdot 10^{-3}$ days. This is in good agreement with the relation derived in the present study, the largest discrepancies occurring for low mass models of large radius (18 per cent). Equation 3.6 also gives periods agreeing with some of the lowest luminosity (1800 $L_\odot$) models of TSB (1979) but deviates significantly when applied to models having large luminosities and radii ($L > 10000\ L_\odot$, $R > 7500\ R_\odot$). Extrapolations of this magnitude are probably not justified however.

In Figure 14, lines of constant mass have been plotted in the (log P, log R) plane for both fundamental mode (solid lines) and overtone (dashed lines) pulsation. Also included in the diagram are observational data points for five stars based on occultation and speckle interferometry data obtained by a number of researchers and compiled by Willson (1982). When several radius estimates were given for a particular star the smallest value was generally selected with the hope that it more nearly represents the photosphere of the object rather than a sampling of the extended atmosphere or circumstellar shell. Two values are given for the radius of each star in Figure 14 based upon whether the stellar disk is assumed to be of uniform brightness or is limb darkened. It should be remembered that the values obtained for the radii of Miras depend upon the wavelength bands used to measure the angular diameters as well as on the assumed distance scale, here based on the K magnitudes of Robertson and Feast (1981; see the discussion of Chapter I), and are still the subject of some uncertainty.

For the radii assumed here, apparently fundamental mode pulsation (with turbulent pressure neglected) is more consistent with observed periods than is overtone pulsation. Furthermore, it does not appear likely

that decreasing the mass of models will be sufficient to allow overtone pulsation. With a lower limit of approximately 0.6 $M_{\odot}$, a consequence of the M_c-L relation of AGB stars, overtone periods may be only slightly larger than those found for the 0.8 $M_{\odot}$ models and certainly not of the magnitude required here.

The inclusion of turbulent pressure has been explored only sparingly in the linear survey because of the time consuming nature of the iteration scheme required, but some conclusions concerning its effects may be drawn. The five turbulent pressure models of Table 7 have been included in Figure 14 and only small changes in the overtone periods are indicated. However, for fundamental mode pulsation, periods have increased significantly, particularly for the low mass models (36 per cent). Apparently turbulent pressure only enhances the difference between modes and produces a wider range of radii at a given fundamental mode period for the masses considered.

Although the results obtained thus far are suggestive, the effects of other assumptions made here, such as time dependent convection, have not been thoroughly explored. It is hoped however, that such problems are of secondary importance when considered in the linear regime. When full amplitude oscillations are allowed it is not likely that the same optimism is justified; in the next chapter these problems will be examined.

Figure 14. Period-mass-radius relations

PMR relations are shown for fundamental mode and first overtone pulsation with turbulent pressure neglected (solid and dashed lines, respectively). Fundamental mode and first overtone periods for five models with turbulent pressure have also been included. Interferometry data from five stars (see Willson, 1982) have been included for comparison; R Leo (313^d), o Cet (332^d), U Ori (372^d), S Vir (388^d), and χ Cyg (407^d).

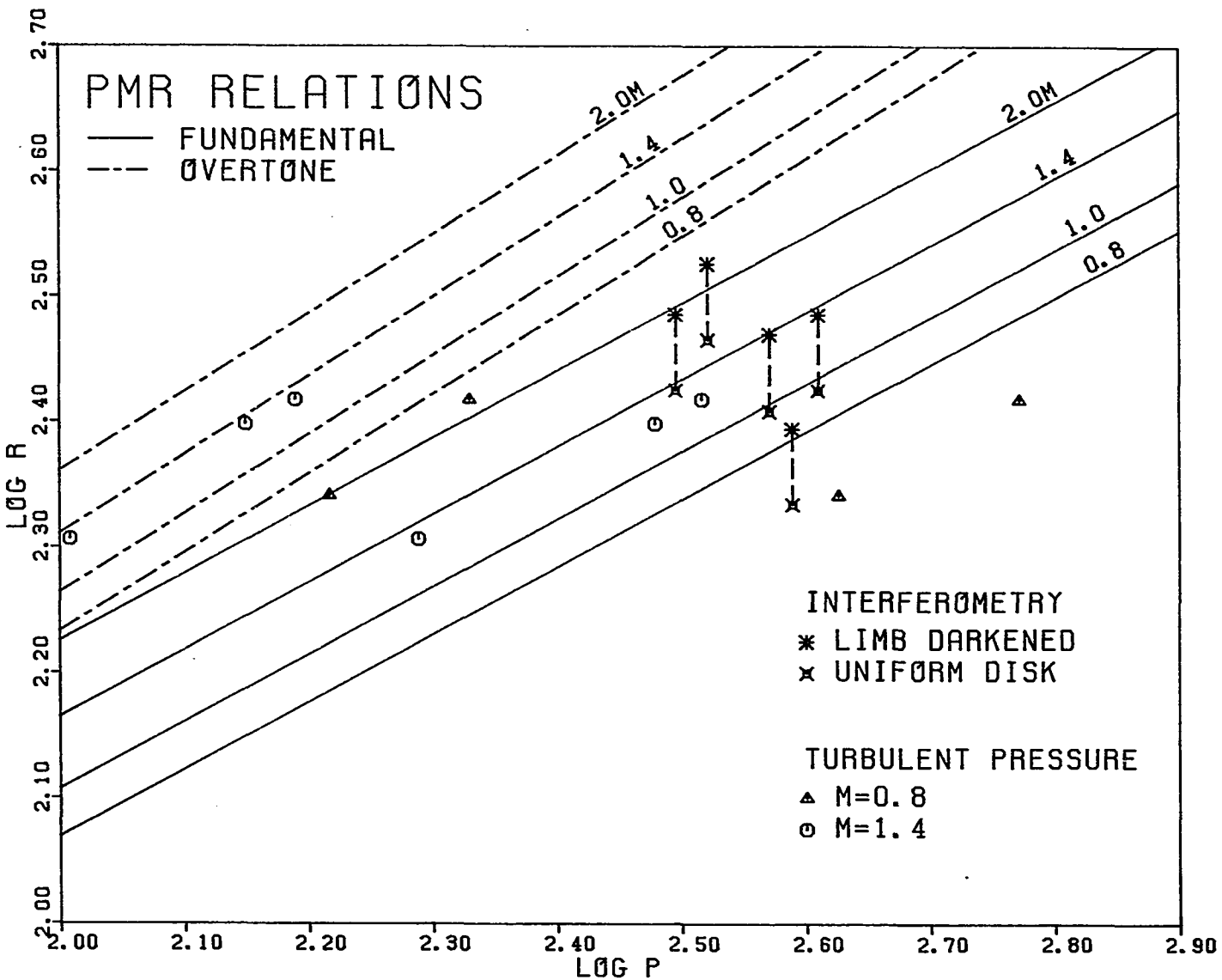
PMR RELATIONS
FUNDAMENTAL
OVERTONE
2.0M
1.4
1.0
0.8
INTERFEROMETRY
LIMB DARKENED
UNIFORM DISK
TURBULENT PRESSURE
M=0.8
M=1.4
LOG R
LOG P
2.00
2.10
2.20
2.30
2.40
2.50
2.60
2.70
2.80
2.90

IV. NONLINEAR PULSATION MODELS

The linear calculations discussed in the previous chapter provide valuable information concerning the periods and stability of several modes of pulsation. Comparison of periods calculated for various values of mass and radius with observed periods and radii indicates that fundamental mode oscillations may dominate in Miras. However, the large visual amplitudes of these stars ($>2^{m}.5$) as well as the radial velocity excursions (perhaps 20 km s^{-1}) mean that the variations are highly nonlinear and that fully hydrodynamic calculations must be carried out in order to understand physically the details of the variability.

A. General Model Considerations

Six models have been investigated using DYNSTAR, a nonlinear, non-adiabatic pulsation code with time dependent convection. Results of the linear stability analysis have already been discussed and presented in Table 7. To test their nonlinear behavior, perturbations in the static structure of these models was accomplished either through self-excitation resulting from computer noise or by the application of linear eigenvectors scaled to moderately large amplitude (typically 2 km s^{-1}).

The first method of perturbation requires substantial amounts of computer time in order to allow the oscillations to obtain limiting amplitude, despite the large growth rates. Although this procedure provides an opportunity to study the approach to limiting amplitude it does not necessarily result in excitation of an appropriate mode. This occurs

because variability may begin when the star occupies a different region of the H-R diagram, perhaps even with a significantly larger mass, and then evolves to the conditions presently observed carrying with it a history of the previous mode of pulsation. Any hysteresis effects that may exist could then result in a mode different from that obtained through self-excitation.

The application of linear eigenvectors to a nonlinear system also has drawbacks. Because the linear and nonlinear eigenvectors are not exactly the same, a number of other modes will also be excited, but presumably with low amplitudes. The presence of multiple modes can be seen in the beating effects present in some of the calculated oscillations.

The time dependent convection formulation used here allows the convective velocity across a zonal interface to lag behind the local instantaneous condition (see Equations 2.22 and 2.23). One characteristic of this approach is that a sudden change in a local temperature gradient from superadiabatic to subadiabatic, which would normally result in the immediate cessation of convective energy transport there, instead induces a gradual decay in the convective velocity. This avoids introducing a discontinuity in the contribution of convection to the overall energy transport. Physically, this results from the inertia of the convective cells. This results in an unusual feature of some of these models, the tendency to refrigerate zones near the top of the convective region during portions of a cycle. Although the instantaneous structure requires that energy be transported solely by radiation when the temperature gradient becomes

subadiabatic, additional energy may be carried away by the lingering convective elements. Trial values of the convective decay parameter (ℓ_τ), other than the standard value of one mixing length, have been considered but were found to alter only the time of onset of the temperature inversion. It is uncertain whether this situation would persist if a more sophisticated theory of time dependence were incorporated.

The use of the diffusion approximation in optically thin zones must also be considered carefully. As has already been mentioned the assumption of diffusive energy transport breaks down when the optical depth is less than unity. To keep the effects of this assumption to a minimum the number of optically thin zones was kept small (usually four) in the hydrostatic models. When full amplitude pulsations are allowed, however, the number of zones in the optically thin region becomes time dependent and periodically includes larger portions of the star, suggesting the need for a better theory of radiative energy transport. Unfortunately, at this time no theory exists that is easily applicable to stellar pulsation studies. The radiative transport of energy through the outermost regions of these stars thus represents a significant uncertainty in the calculations.

In spite of the shortcomings involved in these hydrodynamical calculations the results provide information on features of Mira variable stars not obtainable by other means. In the sections that follow, details of the nonlinear behavior of several models will be discussed, with emphasis placed on the differences resulting from the treatment of convection and the effects of varying the mass.

B. Results of Hydrodynamic Modeling

1. Model 1 - A case neglecting turbulent pressure

The hydrostatic structure of model 1 of Table 7 was perturbed and the resulting time dependent behavior was followed by nonlinear techniques in order to investigate the consequences of neglecting turbulent pressure in pulsation modeling. The results obtained for model 1 may be compared directly with those of model 2, which differs only in that it includes the effects of turbulent pressure.

The bolometric magnitude, radius, and effective temperature for the self-excited sequence are plotted as a function of time and given in Figures 15, 16, and 17, respectively. The model became dominated early by first overtone pulsation with a period of approximately 145 days, very nearly the value of 149 days found from the linear analysis. As the amplitude of the pulsations grew into the nonlinear regime, unstable behavior resulted, however. With the increasing amplitude the average photospheric radius also increased, accompanied by a lengthening of the pulsation period. The increase in radius persisted until two large radial excursions occurred near $2.00 \cdot 10^8$ sec and $2.15 \cdot 10^8$ sec resulting in the loss of all history of first overtone pulsation. With these two bumps, strong minima in both the effective temperature and the luminosity (maximum bolometric magnitude) occurred. Following collapse after the second excursion, amplitudes remained small until a new expansion phase began to develop near the end of the calculation. At this point the stellar structure became sufficiently extreme that prohibitively small time steps were required to follow the pulsations further.

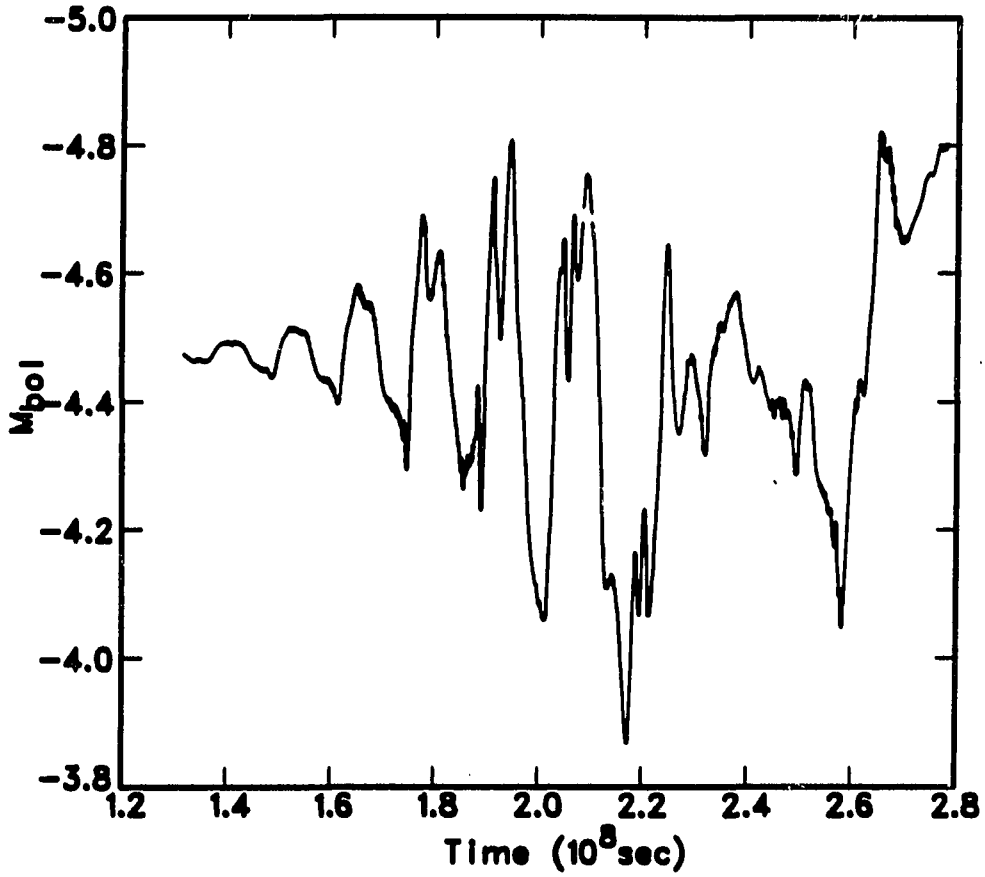

Figure 15. The bolometric light curve for a nonlinear 0.8 $M_\odot$ model without turbulent pressure

For this model (model 1 of Table 7) L = 5000 $L_\odot$, T_e = 3275 K, and ℓ/H_p = 2.66.

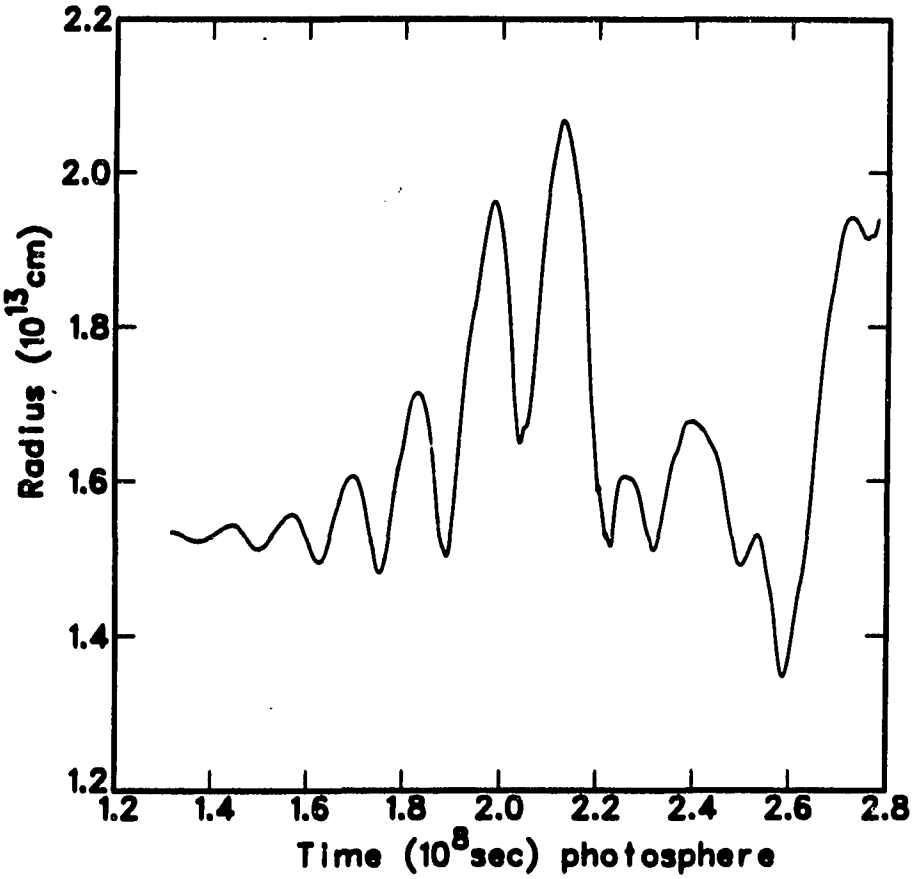

Figure 16. The variation of the photospheric radius with time for a 0.8 $M_\odot$ model without turbulent pressure (model 1 of Table 7)

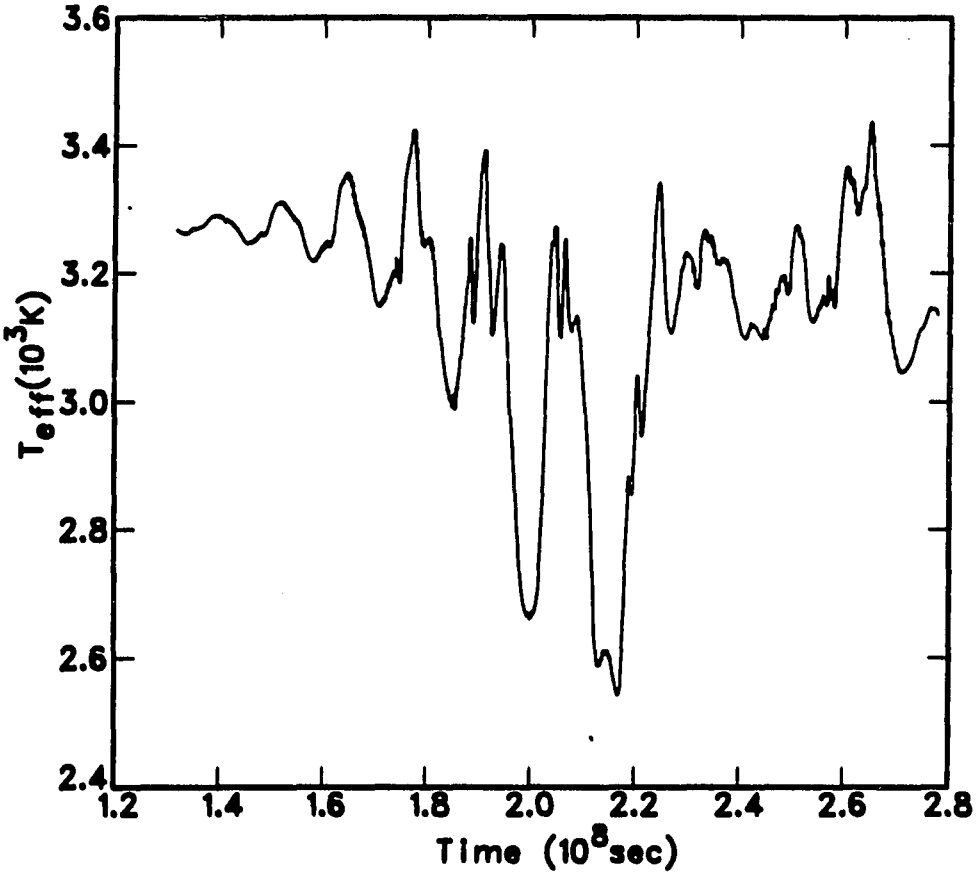

Figure 17. The variation of the effective temperature with time for a 0.8 $M_\odot$ model without turbulent pressure (model 1 of Table 7)

Shortly after the first large excursion at $2.0 \cdot 10^8$ sec the temperature gradient of the outermost layers of the convective region became subadiabatic. This resulted in a rapid decrease in the convective luminosity as can be seen in Figures 18 and 19 for zone 36 (initially at a temperature of 9266 K). In slightly deeper zones a steepening of the temperature gradient resulted in locally large convective luminosities leading to the development of a small temperature inversion. A reversal of radiation flow then occurred as well as a local collapse. In this fashion the energy content of the zone was soon replenished and a more conventional temperature structure was reestablished.

During the early phase of the calculations, while pulsation amplitudes were still small, nearly every zone of the model contributed to the driving. As the oscillations became increasingly nonlinear however, damping regions began to develop. The strongest damping regions were located below the helium ionization zone, where Γ_3-1 is large and constant, and at the top of the envelope. The bulk of the driving during large amplitude oscillations was located in the region of outwardly decreasing Γ_3-1 associated with the zone of partial hydrogen ionization, just as was predicted by the linear analysis.

Figure 20 shows the growth of the envelope kinetic energy to a maximum coinciding with the first of the large radial excursions. Despite the ensuing irregular behavior there is some indication that the damping mentioned is sufficient to quench the large growth rates once nonlinearity has been obtained. For this figure the growth rate has been estimated at $\eta = 1.5$, roughly twice the value determined from the linear study for over-

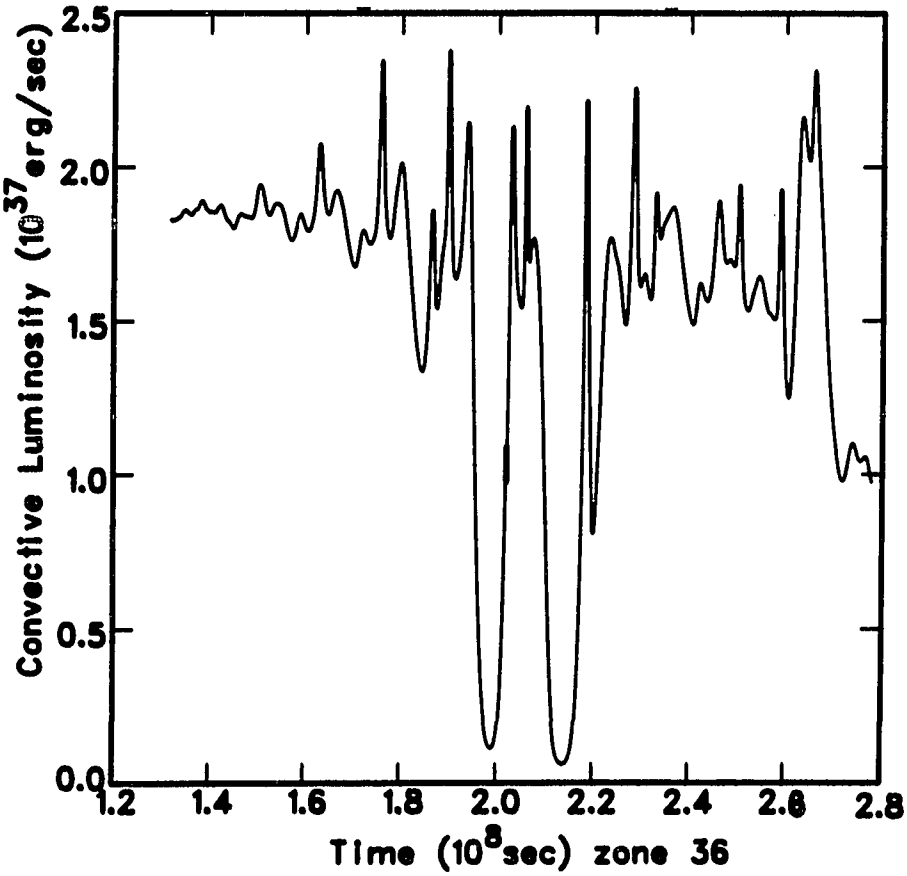

Figure 18. Convective luminosity as a function of time in the hydrogen ionization region with turbulent pressure neglected

The initial, hydrostatic temperature of zone 36 of model 1 was 9266 K.

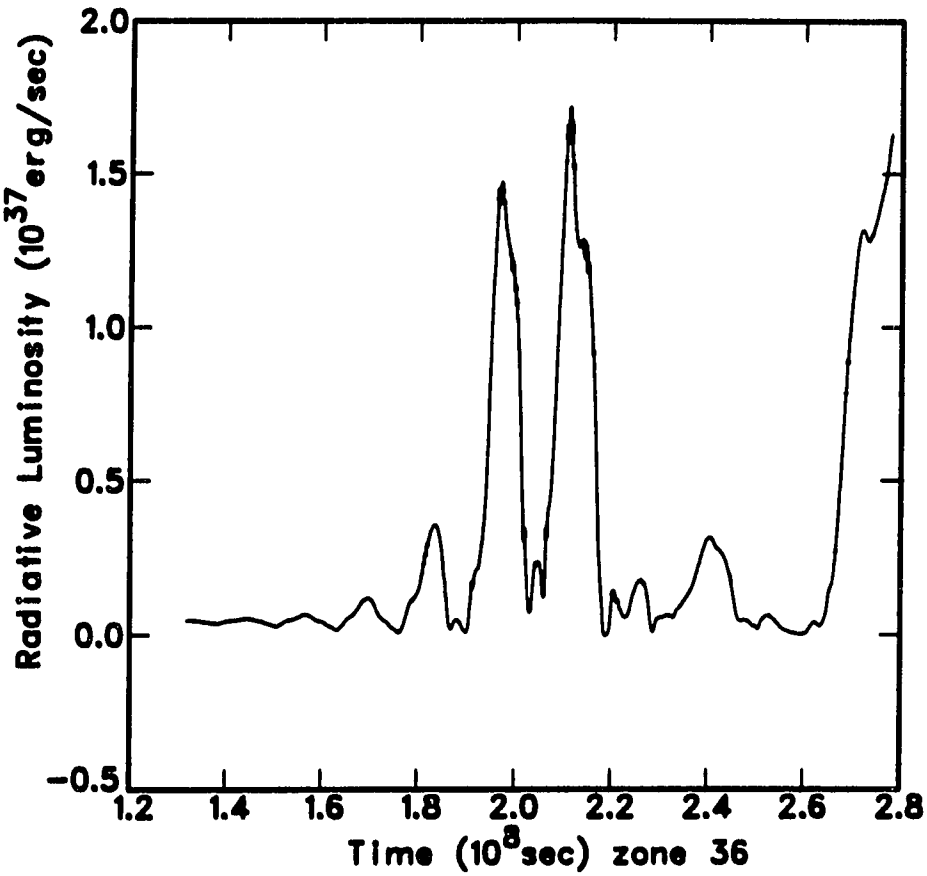

Figure 19. Radiative luminosity as a function of time in the hydrogen ionization region with turbulent pressure neglected (model 1)

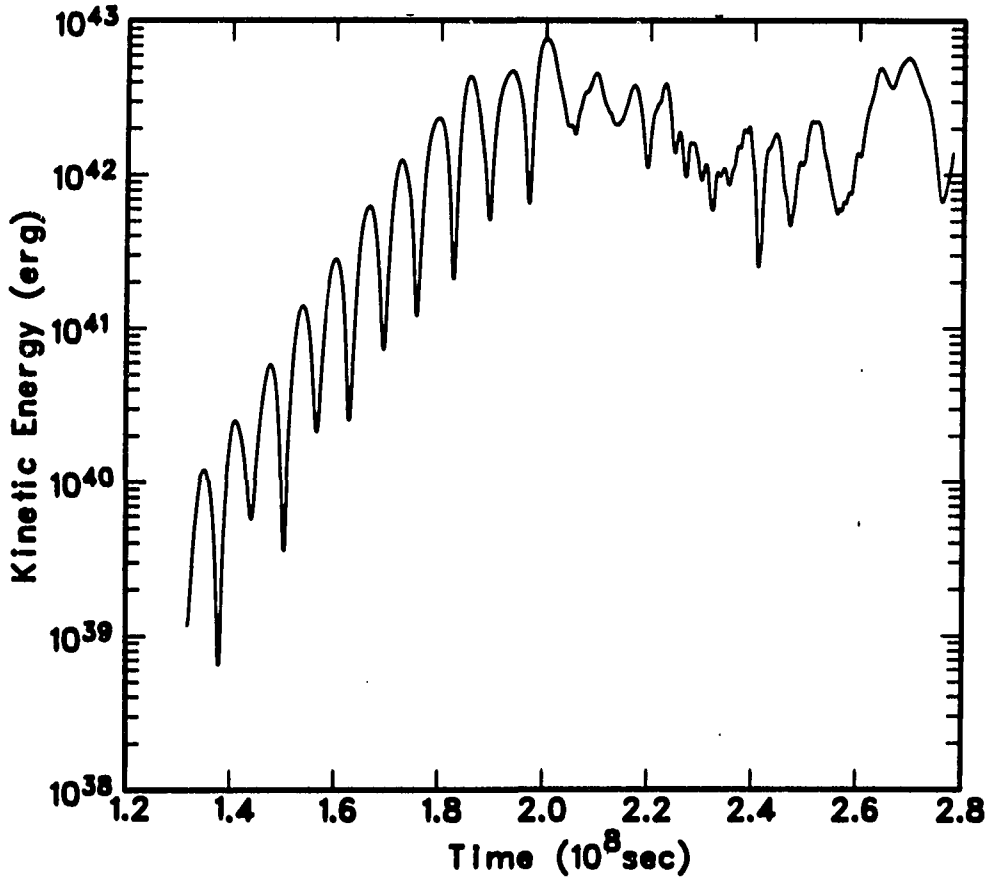

Figure 20. The growth of envelope kinetic energy for a self-excited model without turbulent pressure (model 1)

tone pulsation. In view of the distinct lack of linearity in these models this agreement is quite good.

When a fundamental mode perturbation of 2 km s^{-1} was applied to the same model similar behavior was observed. As before, the average radius of the model increased and the effective temperature decreased due to a net storage of energy. Unfortunately, in this series of calculations it is unclear whether the amplitude would be limited before the outer zones reached escape velocity. When the sequence was terminated because prohibitively small time steps were required to satisfy the energy balance equation, the kinetic energy showed no sign of an approaching upper limit. In light of the rapid turnover demonstrated in the self-excited case the existence of an upper limit still cannot be ruled out, however.

Although no temperature inversions were detected in the fundamental mode calculations, very large local convective luminosities did occur for short periods of time. At one point, zone 29 (having a hydrostatic temperature of $3 \cdot 10^4$ K) reached a peak convective luminosity of $6 \cdot 10^{37}$ erg s^{-1}, compared to an average stellar luminosity of $1.9 \cdot 10^{37}$ erg s^{-1}. A minimum luminosity of $0.2 \cdot 10^{37}$ erg s^{-1} had preceded the large energy output. Such luminosity modulation in radiation and convection, when their sum is properly phased with the radial oscillations, is ultimately responsible for the driving of stellar oscillations.

2. Pulsations in 0.8 $M_\odot$ models including convective turbulence

As already mentioned, model 2 differs from model 1 only in the inclusion of turbulent pressure and the resulting adjustment of ℓ/H_p. Both models 2 and 3 contain turbulent pressure but differ in temperature. Because the

behavior of the two 0.8 $M_\odot$ turbulent pressure models are so similar only model 2 will be described in detail.

Figures 21, 22, and 23 show respectively the bolometric magnitude, radius, and effective temperature as a function of time for the self-excited sequence of calculations. As in model 1, the first overtone dominated pulsations with a period very nearly the same as the one predicted by LNA and with a growth rate roughly twice the value determined by the linear analysis. The node was found to lie near 10^4 K, the top of the region of outwardly decreasing Γ_3-1 in the hydrogen ionization zone. Unfortunately, as in all sequences for 0.8 $M_\odot$ models, numerical difficulties in satisfying the energy balance equation resulted in very small time steps being needed and the calculations were terminated.

Many features of the early phases of the hydrodynamic turbulent pressure models are similar to those of model 1. As before, most zones contribute to pulsational driving during the low amplitude oscillations, but now PdV work done by turbulent pressure adds to the work done by other pressure sources, enhancing the growth rate. However, due to the early termination of the calculations it is unclear whether damping regions of sufficient strength will develop to produce a limiting amplitude before the outer zones reach escape velocity.

Close examination of Figures 21 through 23 reveals the phase lags that exist between the times of minimum photospheric radius and maximum effective temperature and luminosity. Although the linear analysis does predict a lagging of the luminosity maximum behind the time of minimum radius, the delay is much less than the roughly 90° phase lag

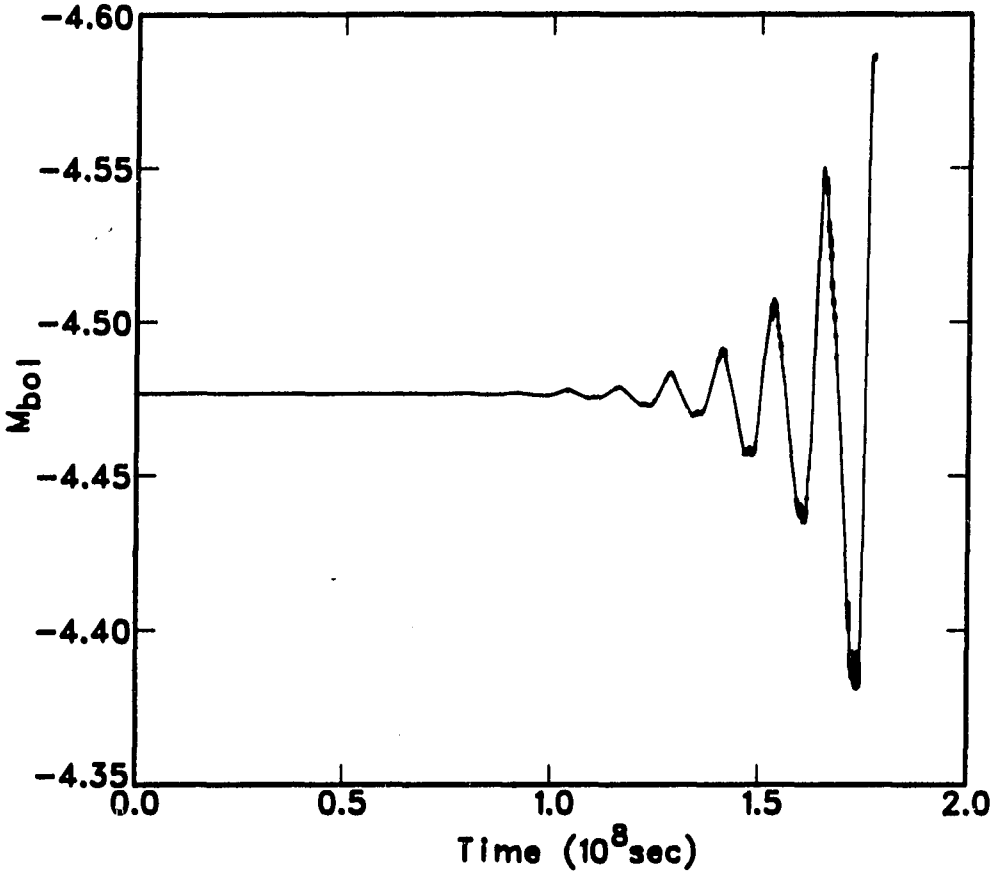

Figure 21. The bolometric light curve for a nonlinear 0.8 $M_\odot$ model with turbulent pressure

For this model (model 2 of Table 7) L = 5000 $L_\odot$, T_e = 3275 K, and ℓ/H_p = 2.88.

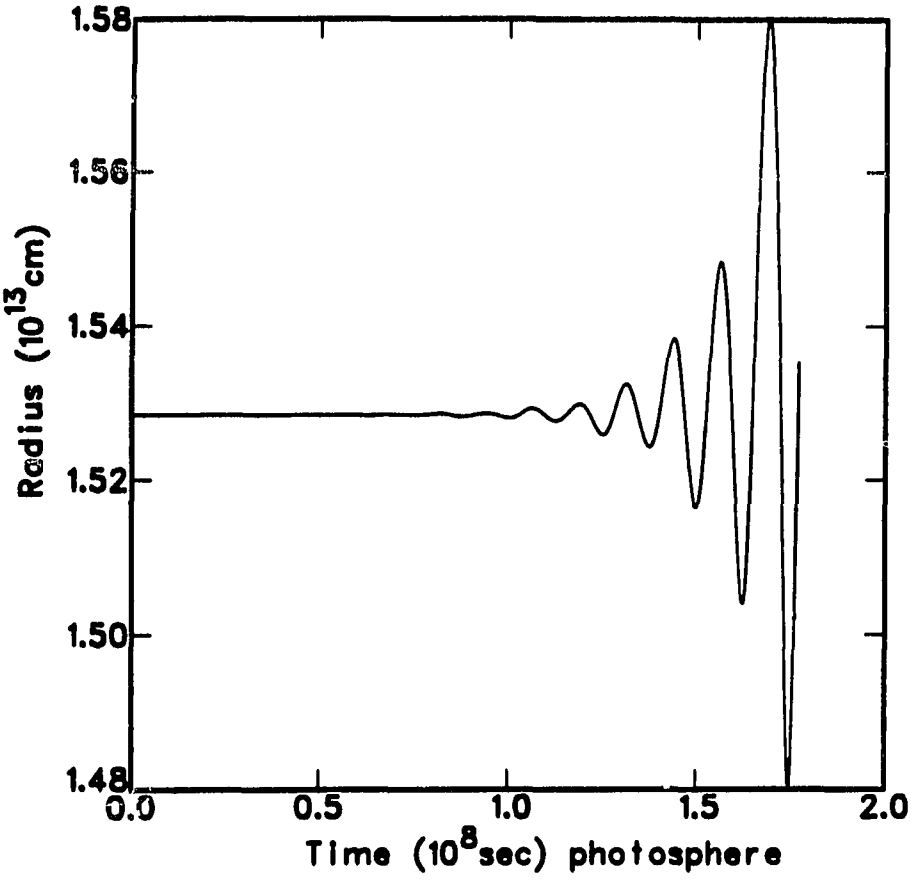

Figure 22. The variation of the photospheric radius with time for a 0.8 $M_{\odot}$ model with turbulent pressure (model 2 of Table 7)

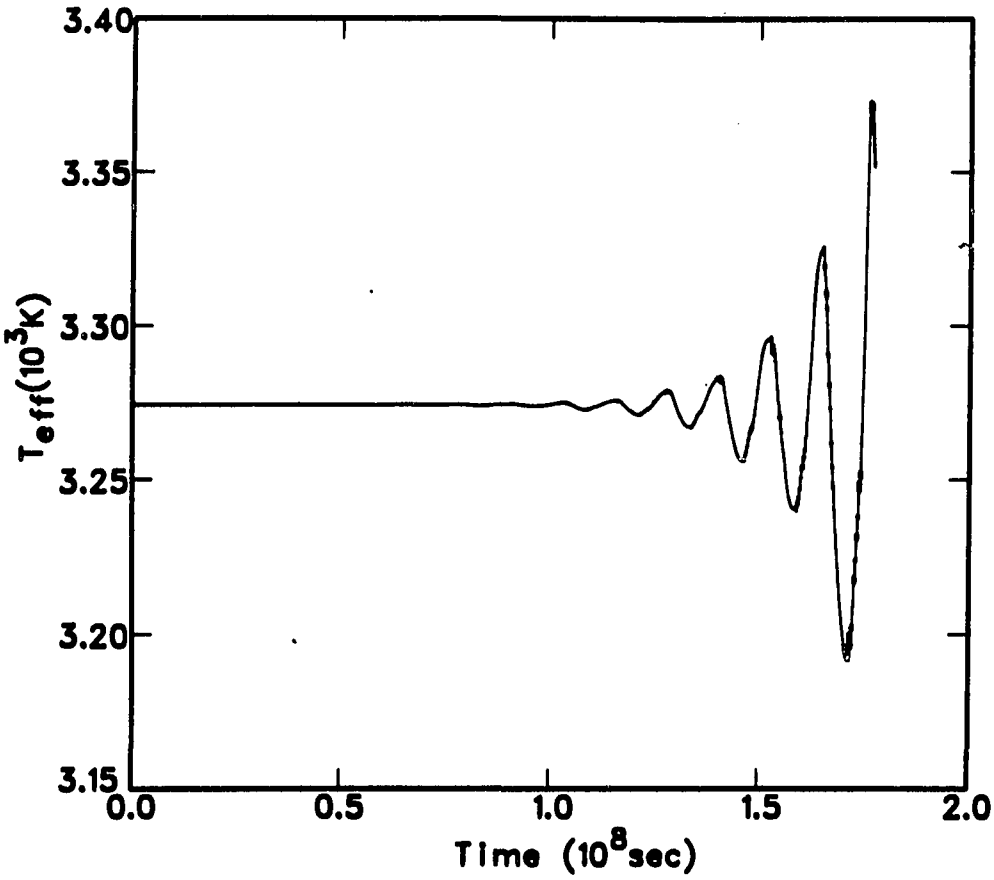

Figure 23. The variation of the effective temperature with time for a 0.8 $M_\odot$ model with turbulent pressure (model 2 of Table 7)

exhibited by the present calculations. The phase lag in the effective temperature is smaller but still significant. The delay in luminosity maximum is easily understood in light of the driving mechanisms discussed previously. To sustain stellar oscillations, energy must be stored during maximum compression and released as expansion begins, forcing the overlying material outward. It is during the release of this energy that the luminosity maximum will occur.

Some important differences between models 1 and 2 are apparent in Figures 15 through 23. As expected from the linear analysis, larger growth rates and longer periods resulted when the effects of turbulent pressure were considered, with the strongest influence occurring during fundamental mode pulsation. The general numerical difficulties encountered with the 0.8 $M_\odot$ model calculations may result from the rapidly increasing amplitudes implied by these large growth rates.

Some evidence may also exist for smoothing of local perturbations by turbulent pressure. The effective temperature curve, as well as the peaks in the bolometric light curve, appear to be less ragged in model 2. This may be the result of increased superadiabaticity during compression of some zones, causing larger convective velocities and therefore larger turbulent pressure contributions. This then opposes the local compression, damping transient oscillations.

3. Pulsation in 1.4 $M_\odot$ models

The nonlinear behavior of the 1.4 $M_\odot$ models differs substantially from the 0.8 $M_\odot$ models described above. The light curves obtained for fundamental mode pulsation in these models possess significantly smaller

amplitudes than was obtained with the lower mass. Most of the important physical parameters also exhibit relatively smooth time dependent variations in contrast to the aperiodic fluctuations evident in many of the 0.8 $M_\odot$ calculations. Here emphasis will be placed on the results obtained for model 4, which may be considered characteristic of those obtained for the other 1.4 $M_\odot$ models.

In Figures 24, 25, and 26 the bolometric magnitude, radius, and effective temperature are given as functions of time for the sequence of calculations resulting from a 2 km s^{-1} fundamental mode perturbation of model 4. It is apparent from these plots that a limiting amplitude for the oscillations has been obtained. Careful examination of the envelope kinetic energy actually shows a small decay in the pulsation amplitude after the initial perturbation, indicating that the system had been overdriven. The period calculated here is approximately 300 days, slightly shorter than the 339 day period determined by the linear study.

Because fairly smooth structural changes occur in the present model, temperature gradients do not suddenly switch between superadiabatic and subadiabatic in regions of strong convective transport, as occurred for the low mass models. This allows a well behaved modulation of the convective luminosity and avoids the propagation of disturbances that may ultimately lead to convergence difficulties (see Figure 27 for zone 27).

With limiting amplitude a balance between driving and damping is implied. The major portion of the driving in this model occurs in the region of partial hydrogen ionization, but with a significant contribution coming from the partial second helium ionization region. This second

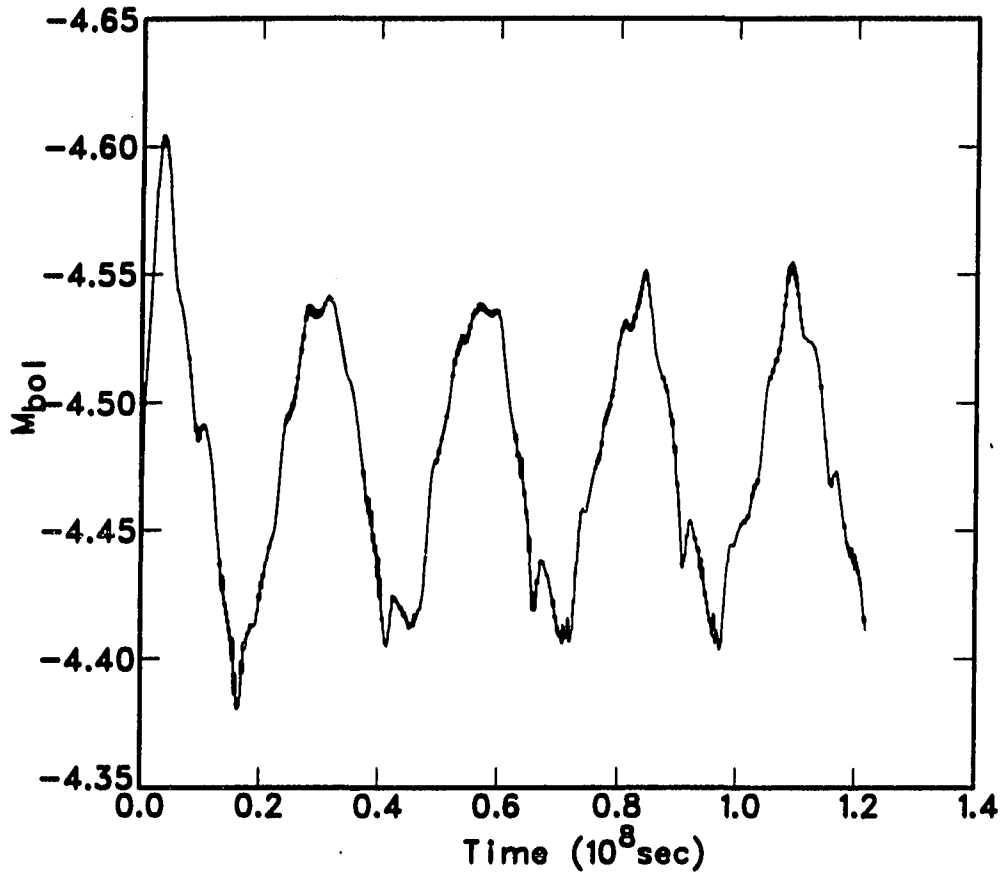

Figure 24. The fundamental mode bolometric light curve for a nonlinear 1.4 $M_\odot$ model (model 4 of Table 7)

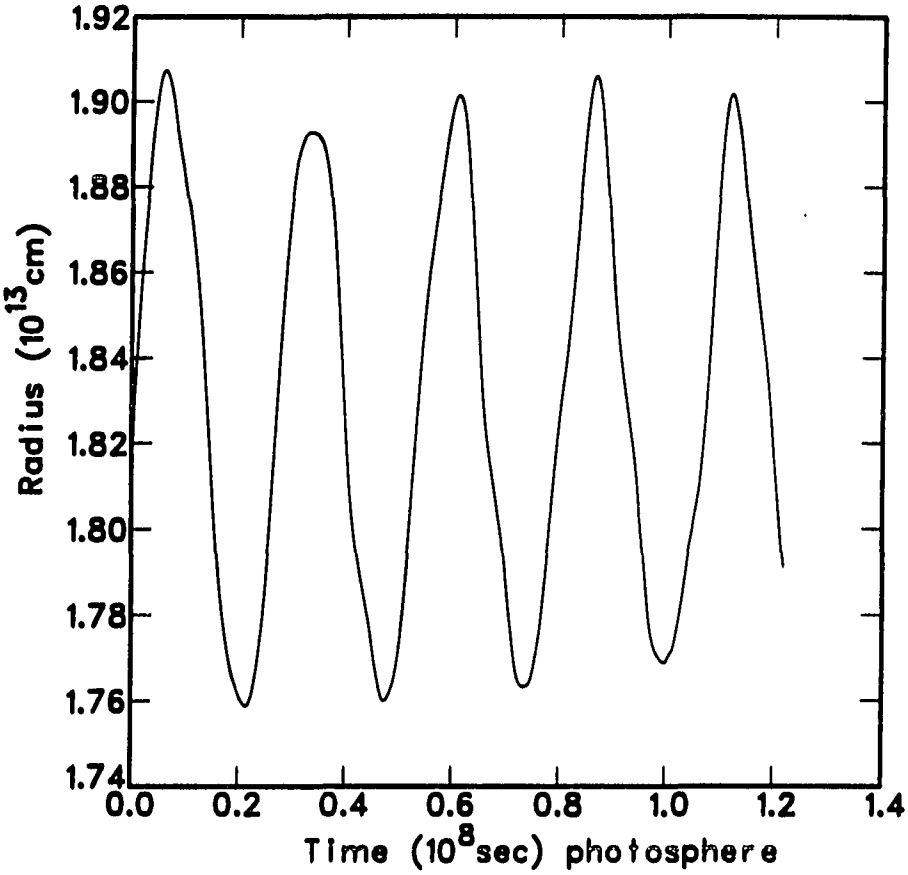

Figure 25. The fundamental mode variation of the photospheric radius with time for a 1.4 $M_{\odot}$ model (model 4 of Table 7)

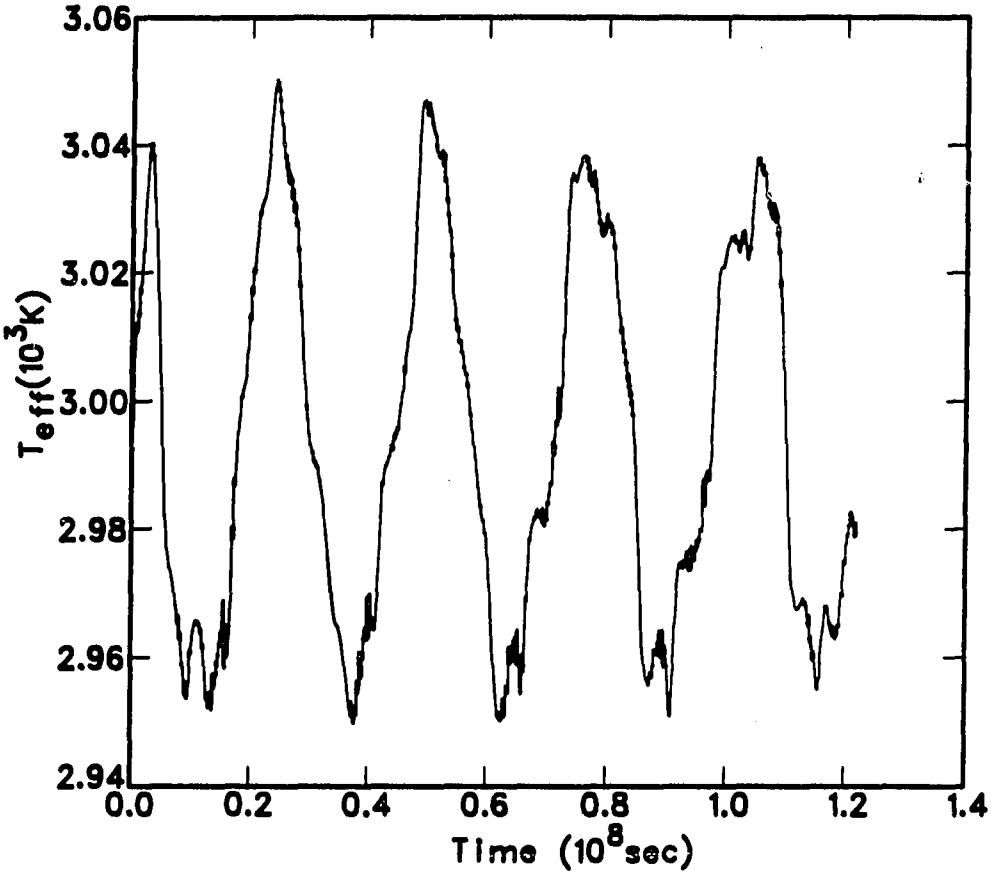

Figure 26. The fundamental mode variation of the effective temperature with time for a 1.4 $M_\odot$ model (model 4 of Table 7)

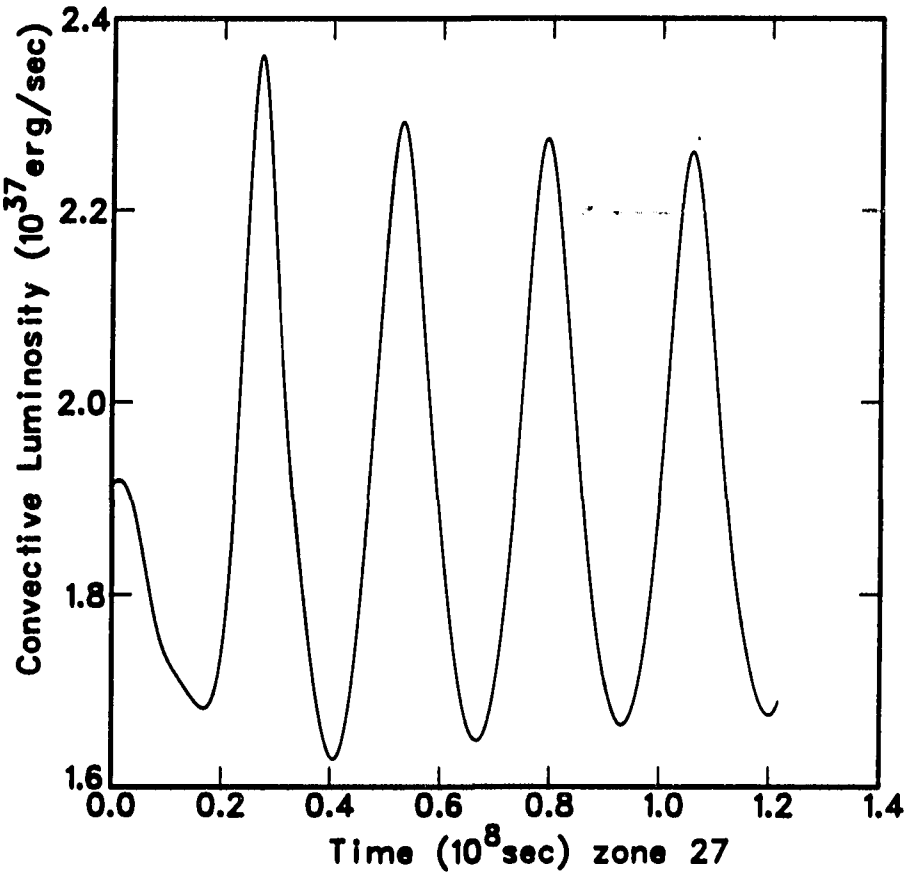

Figure 27. Convective luminosity as a function of time for a typical convective zone in a fundamental mode, 1.4 $M_{\odot}$ model (model 4 of Table 7)

The initial, hydrostatic temperature of zone 27 was approximately 25000 K.

source of driving is entirely absent from the linear analysis. The addition of helium driving in the dynamical calculations probably results from allowing the convective luminosity to vary with time in that region. When convection is assumed to be "frozen in" (as was the case in the linear analysis) it is unable to contribute to the periodic blockage of energy transport through a region, which is necessary to cause pulsation. Because convection is the dominant energy transport mechanism in the region of partial second helium ionization any assumptions concerning convection's time dependent behavior are of critical importance there.

During full amplitude pulsation the regions of major damping are located just above and below the second helium ionization region, with a small contribution to the damping also located in the outermost radiative zones.

Turbulent pressure has been found to contribute significantly to both the driving and damping of pulsations, depending upon zone location. Major turbulent pressure damping regions exist between $1 \cdot 10^5$ K and $6 \cdot 10^4$ K and between $1.5 \cdot 10^4$ K and $1 \cdot 10^4$ K (near the top of the convective region). Driving regions exist throughout most of the remainder of the envelope, with the strongest areas being located between the two turbulent pressure damping regions and above the outermost one. The net effect of including the turbulent pressure contributions is positive: the driving is enhanced.

The mechanism by which turbulent pressure enhances or diminishes driving is difficult to understand, as the arguments are quickly lost in the equations of the convective mixing length theory. However, there is some indication that turbulent pressure damping regions are most likely

to exist near minima in Γ_3-1. This may result because a local zonal compression will increase the superadiabaticity by steepening the temperature gradient. In this way the convective velocity and the corresponding turbulent pressure are increased, resulting in less energy being stored during compression.

C. Model Comparison

Although model 4 (1.4 $M_\odot$) exhibits a stable fundamental mode period of approximately 300 days, the amplitudes of the oscillations are significantly smaller than is observed for Miras. Observations indicate peak-to-peak bolometric amplitudes of approximately $0^m.5$ to 1^m and radial velocity amplitudes of roughly 30 km s^{-1}, compared to the values calculated here of $0^m.15$ and 4 km s^{-1}, respectively. Model 6 (1.4 $M_\odot$) shows slightly larger bolometric magnitude and radial velocity amplitudes ($0^m.25$ and 7 km s^{-1}, respectively) but these are still significantly smaller than those needed to correspond to the Mira variable stars. On the other hand, fundamental mode and first overtone oscillations of models 2 and 3 (0.8 $M_\odot$) have shown very large amplitudes ($\Delta M_{bol} = 1^m.5$ and $\Delta V = 24$ km s^{-1} for fundamental mode pulsation of model 3) before calculations were terminated. Apparently, basic differences exist between the 0.8 $M_\odot$ and 1.4 $M_\odot$ models described here.

As was shown in Chapter III, the growth rates for fundamental mode pulsation are well correlated with the degree to which the pulsations are nonadiabatic, as measured by the ratio of the Kelvin time to the pulsation period (see Figure 13 and Equation 3.5). The nonlinear behavior of the

models also seems to be dependent upon the amount of nonadiabaticity. For models 2 and 3 the large growth rates indicate very nonadiabatic pulsation and correspondingly large amplitudes. For model 1 the neglect of turbulent pressure resulted in a lower growth rate. Although large amplitudes were also obtained in this case and limiting values were eventually reached, these oscillations were very irregular. Models 4, 5, and 6, with their lower growth rates and correspondingly more nearly adiabatic pulsations, obtained small amplitudes.

The dependence of nonlinear behavior on the amount of nonadiabaticity may be influenced by a number of approximations. The treatment of the surface boundary conditions does not take into consideration losses due to kinetic energy transport across the outer boundary. Such transport, in the form of running waves and mass loss, is known to occur. Although the consequences of assuming that kinetic energy transport is insignificant at the surface are difficult to evaluate,it is apparent that this does involve a nonadiabatic feature of these stars. The approximation of diffusive radiation transport in optically thin regions is also likely to introduce errors near the surface.

Perhaps the most significant approximation made in the nonlinear study, however, involves the method of treating time dependent convection. Because convection plays such a dominant role in the energy transport it is likely to be intimately linked to the degree of nonadiabaticity. Obviously stability, and ultimately the limiting amplitudes obtained, are strongly coupled to the phasing of convection, radiation, and pulsation. If the amount of energy transported by convection through a driving region

at any given phase is incorrect, the amount of driving will also be incorrect, resulting in amplitudes that may be too large or too small.

Considering the apparent dependence of pulsation amplitudes on the treatment of time dependent convection and on the boundary conditions used it seems premature at this time to expect that the present calculations closely mimic the behavior of actual stars. It may be more appropriate to look upon this study as a preliminary examination of the nonlinear nature of Mira variable star pulsations.

V. SUMMARY AND CONCLUSIONS

In this work an extensive mapping of the Mira instability region of the H-R diagram has been carried out using linear models. If the current estimates of mass and radius prove to be correct, these results seem to indicate that fundamental mode pulsations are consistent with the known properties of these objects, while first overtone oscillations apparently require masses that are too low to be compatible with current evolutionary models.

Results of a preliminary survey using nonlinear models is less conclusive. For 0.8 $M_\odot$ models with convective turbulent pressure included, limiting amplitude was not obtained for any mode of pulsation. The calculations begun with excitation resulting from machine noise produced first overtone pulsation, with growth rates roughly twice those predicted by the linear analysis. Unfortunately, these oscillations showed no sign of stabilizing at a finite amplitude. The turbulent pressure 0.8 $M_\odot$ models initially perturbed by a 2 km s^{-1} fundamental mode eigenvector exhibited very rapid growth rates leading ultimately to convergence difficulties and termination of the calculations.

The nonlinear calculations involving 1.4 $M_\odot$ models did obtain limiting amplitudes when perturbed by fundamental mode eigenvectors. In these cases the periods were found to be very near the values obtained from the linear analysis, but with radial velocity and bolometric magnitude variations much smaller than those observed for Miras.

Effects resulting from the inclusion of turbulent pressure were generally found to be small when infinitesimal oscillations were considered.

It was determined that the effects of turbulent pressure were most significant for models having very nonadiabatic pulsations, but that they decreased rapidly when adiabaticity was approached. By comparing the ratio of the Kelvin time to the fundamental mode pulsation period, an estimate of the degree to which models deviated from adiabaticity could be obtained. For the lowest mass models, where the deviation was found to be the largest, fundamental mode pulsation periods were increased by up to 30 per cent when turbulent pressure was included. For the most massive models the periods were much less affected.

The behavior of the fully hydrodynamic calculations appears to be intimately linked to the amount of nonadiabaticity present in the models. In the highly nonadiabatic low mass models, pulsation amplitudes became very large, with a limiting amplitude (although aperiodic) light curve resulting only when turbulent pressure was neglected. For the more massive stars the amplitudes of fundamental mode pulsation were much smaller than observed, but the light curves were more periodic than those of the low mass models.

Significant improvements still need to be made if we hope to fully understand Mira variable stars. Because behavior and nonadiabaticity are so closely related, a good treatment of energy transport is certainly required. Near the surface both radiation (poorly treated there by the diffusion approximation) and kinetic energy transport must play major roles in the time dependent structure, while in the interior, energy transport is dominated by convection, influencing the driving and damping of pulsations.

Of the various transport mechanisms the largest uncertainties arise from the treatment of convection. Attempts have been made here to alleviate some of the inconsistencies inherent in the standard form of the mixing length theory: in all models, an averaging of the opacities of rising and falling convective elements has been included, the effects of turbulent pressure have been investigated in a number of cases, and a time-dependent formulation for modulating convective velocities in the nonlinear calculations has been added.

Although a number of modifications have been made in the mixing length theory, many questions still remain concerning its validity. Convection is certainly a three dimensional phenomenon requiring complex hydrodynamic calculations to follow the energy transport in detail. Unfortunately, at this time we are forced to assume that the transport may be adequately approximated by a one dimensional, free parameter theory. Yet, in spite of the large amount of work still needed, it is reassuring to note that the results obtained thus far seem to describe some of the important features of these objects.

VI. REFERENCES

Abell, G. O., and Goldreich, P. 1966, Pub. Astr. Soc. Pacific 78, 232.

Barkat, Z., and Tuchman, Y. 1980, Ap. J., 237, 105.

Beavers, W. I., Eitter, J. J., Dunham, D. W., and Stein, W. L. 1980, A. J., 85, 1505.

Böhm-Vitense, E. 1958, Z.f. Ap., 46, 108.

Bonneau, D., Foy, R., Blazit, A., and Labeyrie, A. 1982, Astr. Ap. 106, 235.

Cahn, J. H. 1980, Sp. Sci. Rev., 27, 457.

Cahn, J. H., and Wyatt, S. P. 1978, Ap. J., 221, 163.

Castor, J. I. 1971, Ap. J., 166, 109.

Clayton, D. D. 1968, Principles of Stellar Evolution and Nucleosynthesis (New York: McGraw-Hill).

Clayton, M. L., and Feast, M. W. 1969, M.N.R.A.S., 146, 411.

Cox, J. P. 1980, Theory of Stellar Pulsation (Princeton, N.J.: University Press).

Cox, J. P., and Giuli, R. T. 1968, Principles of Stellar Structure (New York: Gordon and Breach), 2 vols.

Deupree, R. G. 1979, Ap. J., 234, 228.

Eggen, O. 1975, Ap. J., 195, 661.

Faulkner, D. J. 1970, Ap. J., 162, 513.

Feast, M. W. 1963, M.N.R.A.S., 125, 367.

Fernie, J. D., and Brooker, A. A. 1961, Ap. J., 133, 1088.

Fox, M. W., and Wood, P. R. 1982, Ap. J., 258, in press.

Glass, I. S., and Feast, M. W. 1981, M.N.R.A.S., 198, 199.

Gerhz, R. D., and Woolf, N. 1971, Ap. J., 165, 285.

Henyey, L., Vardya, M. S., and Bodenheimer, P. 1965, Ap. J., 142, 841.

Hill, S. J., and Willson, L. A. 1979, Ap. J., 229, 1029.

Hinkle, K. H., and Barnes, T. G. 1979, Ap. J., 234, 548.

Iben, I. Jr., and Truran, J. W. 1978, Ap. J., 220, 980.

Johnson, H. J. 1966, Ann. Rev. Astr. and Ap., 4, 193.

Johnson, H. R., Bernat, A. P., and Krupp, B. M. 1980, Ap. J. Suppl., 42, 501.

Kamijo, F. 1963a, Pub. Astr. Soc. Japan, 14, 271.

_____. 1963b, Pub. Astr. Soc. Japan, 15, 1.

_____. 1963c, Pub. Astr. Soc. Japan, 15, 440.

Keeley, D. A. 1970a, Ap. J., 161, 643.

_____. 1970b, Ap. J., 161, 657.

Knapp, G. R., Phillips, T. G., Leighton, R. B., Lo, K. Y., Wannier, P. G., Wootten, H. A., and Huggins, P. J. 1982, Ap. J., 252, 616.

Kukarkin, B. V. et al. 1969-1976, General Catalogue of Variable Stars (3d ed.; Moscow: USSR Acad. Sci.).

Kwok, S., Purton, C. R., and Fitzgerald, P. M. 1978, Ap. J., 219, L125.

Labeyrie, A., Koechlin, L., Bonneau, D., Blazit, A., and Foy, R. 1977, Ap. J., 218, L75.

Langer, G. E. 1969, Ph.D. thesis, University of Colorado.

Latour, J. 1970, Astr. Ap. 9, 277.

Lucy, L. B. 1967, A. J., 72, 813.

O'Dell, C. R. 1966, Ap. J., 145, 487.

Osterbrock, D. E. 1974, Astrophysics of Gaseous Nebulae (San Francisco: Freeman).

Paczynski, B. 1969, Acta Astr., 19, 1.

Paczynski, B., and Ziolkowski, J. 1968, Acta Astr., 18, 255.

Reimers, D. 1975, Problems in Stellar Atmospheres and Envelopes, ed. Baschek, B., Kegel, W. H., Traving, G. (Berlin: Springer-Verlag), 229.

Ridgway, S. T., Wells, D. C., and Joyce, R. R. 1977, A. J., 82, 414.

Ridgway, S. T., Joyce, R. R., White, N. M., and Wing, R. F. 1980, Ap. J., 235, 126.

Robertson, B.S.C., and Feast, M. W. 1981, N.M.R.A.S., 196, 111.

Ross, J. E., and Aller, L. H. 1976, Science, 191, 1223.

Roxburgh, I. W. 1967, Nature, 215, 838.

Salpeter, E. E. 1971, Ann. Rev. Astr. and Ap., 9, 127.

Scargle, J. D., and Strecker, D. W. 1979, Ap. J., 228, 838.

Schönberner, D. 1979, Astr. Ap., 79, 108.

_____. 1981, Astr. Ap., 103, 119.

Smith, R. L., and Rose, W. K. 1972, Ap. J., 176, 395.

Sparks, W. M., and Kutter, G. S. 1972, Ap. J., 175, 707.

Sweigert, A. V., and Gross, P. G. 1978, Ap. J. Suppl., 36, 405.

Tsuji, T. 1978, Pub. Astr. Soc. Pacific, 30, 435.

Tuchman, Y., Sack, N., and Barkat, Z. 1978, Ap. J., 219, 183.

_____. 1979, Ap. J., 234, 217.

Willson, L. A. 1981, Effects of Mass Loss on Stellar Evolution, ed. Chiosi, C., and Stalio, R. (Dordrecht: D. Reidel), 353.

_____. 1982, preprint.

Willson, L. A., Wallerstein, G., and Pilachowski, C. A. 1982, N.M.R.A.S., 192, 483.

Wood, P. R. 1974, Ap. J., 190, 609.

Wood, P. R., and Cahn, J. H. 1977, Ap. J., 211, 499.

Wood, P. R., and Zarro, D. M. 1981, Ap. J., 247, 247.

VII. ACKNOWLEDGMENTS

I wish to thank Arthur N. Cox for many valuable suggestions during the course of this project as well as for his hospitality during my stay at Los Alamos National Laboratory where these calculations were carried out. I would also like to thank Julius H. Cahn for providing an analytic fit to the Ross-Aller opacity tables, Stephen W. Hodson for assistance with many computational problems, and Lee Anne Willson for suggesting this problem and supervising my work. Finally, I wish to thank my parents for their continuous support and encouragement during school and otherwise.